Supporting Information

Rigidity Matters: Hydrogen Bonding and Inner Filter Effect Govern Selective Sensing of 4-Nitrophenol by Coumarin[4]arenes

Prabukumar Balakrishnan, Venkatakrishnan Parthasarathy*

Department of Chemistry, Indian Institute of Technology Madras, Chennai – 600 036, India

---

Table of Contents

Sl. No.	*Contents*	*Page no.*
1.	General Methods and Materials	S2
2.	Experimental details and Characterization	S3-S6
3.	^{1}H and ^{13}C NMR spectral scans	S7-S11
4.	Absorption and Emission Spectra	S12-S20
5.	Competitive Experiment	S21-S22
6.	Lifetime and LOD Experiment	S23-S24
7.	^{1}H NMR Titration studies	S25-S29
8.	Binding constant estimation from fluorescence titrations	S30
9.	Variable low-temperature ^{1}H NMR experiment	S31
10.	^{1}H DOSY Experiment	S32
11.	Calculation of the Hydrodynamic radii	S32-S34
12.	Experimental details of detection on paper/TLC	S34-S35
13.	Performance comparison table of macrocyles towards NA sensing	S36
14.	References	S37

1. General Methods and Materials

Reactions were performed in an oven dried round bottom flasks under nitrogen gas atmosphere. Solvents were dried using standard procedures unless otherwise mentioned.[1] Toluene was distilled from sodium, diethyl ether and THF from sodium/benzophenone under N_2 gas atmosphere. Chloroform and methylene chloride were distilled on calcium hydride. Solvents used for extraction and purification were technical grade and distilled. All the other chemicals were obtained from Aldrich, Acros, Avra, Alfa-Aesar and used as received unless otherwise indicated. The reactions were monitored by thin-layer chromatography (TLC) using silica-gel (60 F254) plates and compounds were visualized under UV light. Column chromatography was performed on silica gel (100-200 mesh). Melting points were measured on samples in open capillary tubes and were corrected. The infrared spectra of compounds were recorded on a JASCO FT/IR-4100 Fourier transform infra-red spectrometer. The wave numbers of recorded IR signals are quoted in cm^{-1}. ^1H and ^{13}C NMR spectra were obtained at 25 °C using a Bruker AV-400 & AV-500 MHz FT-NMR spectrometer in deuterated solvent $CDCl_3$ with TMS as an internal reference, unless otherwise stated. All the chemical shifts are reported in parts per million (ppm, δ). Coupling constants (J) are given as absolute values; reported in Hertz (Hz). Proton spectral multiplicities are abbreviated as follows s: singlet, d: doublet, t: triplet, m: multiplet, q: quartet. Proton NMR data are expressed as chemical shift in parts per million (ppm, δ) relative to residual solvent peak $CDCl_3$: ^1H, δ = 7.26; ^{13}C, δ = 77.16, respectively; and TMS as internal standard. High resolution mass spectra (HRMS) were recorded on Q-TOF Micro mass spectrometer. UV-visible absorption spectra were recorded on a Agilent Technologies Cary - 8454 UV-Vis diode-array spectrophotometer using distilled (dry) solvents. Photoluminescence spectra were recorded on a Horiba Fluoromax-4 Spectrofluorometer using distilled (dry) solvents.

2. Experimental Section

2.1 Detailed Synthetic Procedure and Characterization Data

2.1.1 General procedure for the preparation of C-alkyl tetramethoxyresorcinarenes 2a-b

The macrocycles **2a-b** were synthesized as per our previous report and their characterization data were found in agreement. The compounds **2a-b** were synthesised using modified literature procedure as given below.

To a solution of 3-methoxyphenol (1.0 g, 8.06 mmol) and the corresponding aldehyde (8.06 mmol) in anhydrous dichloromethane (10 mL) under nitrogen gas atmosphere, boron trifluoride–diethyl ether (2.4 g, 16.93 mmol) was introduced at 0 °C with a flow rate of 0.5-1 mL/min (first half volume with 0.5 mL/min and rest half with 1 mL/min) dropwise to the reaction mixture while maintaining the internal temperature between 5-10 °C throughout the addition. After stirring the reaction mixture further at 0 °C for 30 min, it was then warmed to room temperature and stirred for the next 2 h, quenched with water (10 mL). The crude was extracted with dichloromethane and finally washed with brine solution. The extracted organic layer was dried over anhydrous $MgSO_4$, and the excess solvent was removed under vacuum to yield a dark red oil. The crude was dissolved in a minimum amount of hot methanol and sonicated to afford a white precipitate. The solids obtained were filtered at room temperature, washed with cold methanol, and dried to give pure **2a-b** as a white solid.

2,8,14,20-Tetraisopropyl-4,10,16,22-tetrahydroxy-6,12,18,24-tetramethoxycalix[4]arene (2a):

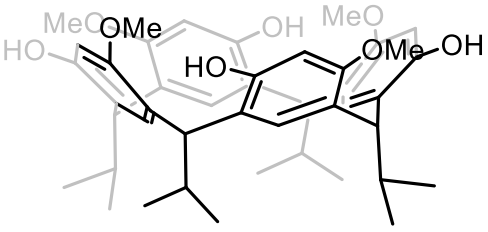

Yield: 0.69 g, 48%. ^{1}H NMR ($CDCl_3$, 500 MHz) δ 7.51 (s, 4H), 7.20 (s, 4H), 6.36 (s, 4H), 3.86 (d, J = 11.35 Hz, 4H), 3.82 (s, 12H), 2.82-2.74 (m, 4H), 0.94 (t, J = 8.7 Hz, 24H). ^{13}C {^{1}H} NMR ($CDCl_3$, 125 MHz) δ 154.0, 153.3, 124.6, 124.5, 100.4, 56.0, 41.8, 30.7, 21.8, 21.7.

2,8,14,20-Tetraisobutyl-4,10,16,22-tetrahydroxy-6,12,18,24-tetramethoxycalix[4]arene (2b):

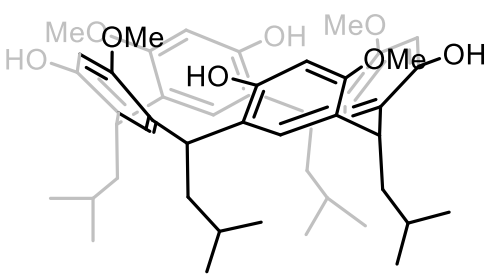

Yield: 12.1 g, 78%; ^{1}H NMR ($CDCl_3$, 500 MHz) δ = 7.52 (s, 4H), 7.23 (s, 4H), 6.37 (s, 4H), 4.43 (t, *J* = 8.5 Hz, 4H), 3.85 (s, 12H), 2.10 (t, *J* = 7.5 Hz, 8H), 1.47 (m, 4H), 0.98 (dd, *J* = 6.6, 4.8 Hz, 24H) ppm; ^{13}C {^{1}H} NMR ($CDCl_3$, 125 MHz) δ = 153.8, 153.1, 124.9, 124.7, 124.2, 100.2, 56.0, 43.2, 30.8, 26.2, 23.0, 22.9 ppm;

2.1.3 General procedure for the synthesis of coumarin[4]arene[1,2,3]

The macrocycles **1a-b** were synthesized as per our previous report and their characterization data were found in agreement. The compounds **1a-b** were synthesised using the procedure as given below.

To a solution of tetramethoxyresorcinarenes **2a-b** (1.0 mmol) in anhydrous toluene (10 mL) under nitrogen gas atmosphere at 90 °C, Meldrum's acid (4.05 mmol) was added, and the reaction mixture was heated for 12 h with constant stirring. The mixture was then cooled to room temperature, and resulted precipitates were filtered and washed with toluene (10 x 2 mL) and dried to yield their respective half malonic acid as a white solid. The isolated crude solid was taken to the next step without any further purification.

The isolated crude solid was added to a freshly prepared solution of Eaton's reagent (10 mL) under nitrogen gas atmosphere at 50 °C and heated with stirring for 10 h. The mixture was then cooled to room temperature and poured into crushed ice (100 g). The resultant off-white precipitates were filtered and dried. The crude product was recrystallized with acetonitrile/DCM to yield **1a-b** as white solid.

***C*-isopropyl coumarin[4]arene (1a):**

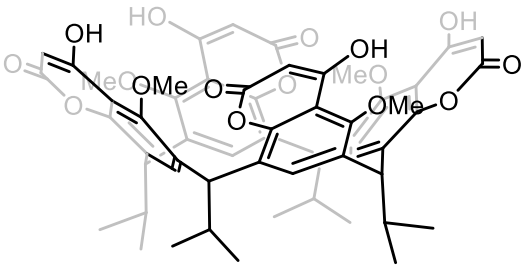

Yield: 0.870 g, 93%. Mp 250-252 °C. FT-IR (KBr, cm^{-1}): 3282, 3051, 2986, 2835, 1716, 1648, 1587, 1421, 1165, 894, 725. ^{1}H NMR ($CDCl_3$, 500 MHz) δ 10.02 (bs, 4H), 7.39 (s, 4H), 5.70 (s, 4H), 4.68 (d, *J* = 10.97 Hz, 4H), 4.18 (s, 12H), 2.41-2.34 (m, 4H), 0.94 (dd, *J* = 6.4, 46.74 Hz, 24H). ^{13}C {^{1}H} NMR ($CDCl_3$, 125 MHz) δ 165.6, 162.3, 153.7, 150.8, 131.1, 129.3, 128.1, 108.6, 93.7, 65.2, 41.4, 33.0, 21.4, 21.2. HRMS (ESI-TOF) *m/z:* $[M + H]^+$ calcd for $C_{56}H_{57}O_{16}$ 985.3647, found 985.3635.

C-Isobutyl coumarin[4]arene (1b):

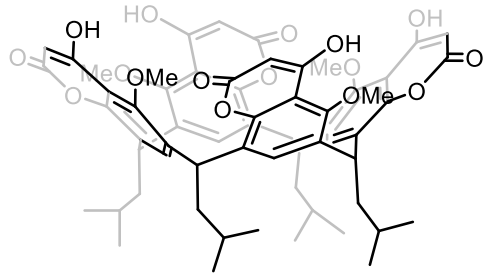

Yield: 3.62 g, 92%; IR (KBr): 3275, 2956, 2869, 1719, 1654, 1617, 1586, 1459, 1387, 1303, 1265, 1167, 1093, 989, 834, 736 cm^{-1}; ^{1}H NMR ($CDCl_3$, 500 MHz) δ = 9.83 (brs, 4H), 6.87 (s, 4H), 5.70 (s, 4H), 4.85 (t, *J* = 7.5 Hz, 4H), 3.97 (s, 12H) 1.95-1.89 (m, 8H), 1.81-1.76 (m, 4H), 1.56-1.50 (m, 4H), 1.03 (dd, *J* = 22.5, 6.5 Hz, 24H) ppm; ^{13}C {^{1}H} NMR ($CDCl_3$, 125 MHz) δ = 165.3, 161.8, 152.8, 150.4, 131.9, 129.1, 128.5, 108.6, 93.9, 64.2, 44.0, 34.3, 26.2, 22.8, 22.7 ppm; ESIHRMS: calcd for $C_{60}H_{64}O_{16}$+H 1041.4273, found 1041.4286; Mp 235 °C.

2.2 Estimation of fluorescence quantum yield

The fluorescence quantum yields (Φ_F) of compounds **1a** and **1b** were determined using the relative method, with 9,10-diphenylanthracene (Φ_R = 0.97) as the reference standard. The quantum yield was calculated by employing the equation provided below:

$$\phi_F = (\phi_R) \times \left(\frac{Is}{I_R}\right) \times \left(\frac{OD_R}{ODs}\right) \times \frac{n_S^2}{n_R^2}$$

where ϕ denotes the quantum yield, I indicate the integrated area of fluorescence intensity, OD refers to the optical density, and n represents the refractive index of solution. The subscript 'R' represents the reference fluorophore, whose quantum yield is known, while the subscript 'S' corresponds to the sample fluorophore, for which the quantum yield is to be determined."

2.3. Estimation of limit of detection (LOD)

The limit of detection (LOD) was determined using the fluorescent titration method, applying the following equation:

LOD = 3σ/K

Here, σ represents the standard deviation of 7 blank measurements, while K denotes the slope of the corresponding linear plot.

2.4. Estimation of quenching constant

The fluorescence quenching was determined using the Stern-Volmer equation

$$\frac{I_0}{I_0 - I} = 1 + K_{SV}[Q]$$

Where I_0 and I are the fluorescence intensities of **1a/1b** in the absence and presence of nitroaromatics respectively, [Q] denotes the concentration of the nitroaromatics and K_{SV} represents the Stern-Volmer quenching constant. The association constant is determined using modified Stern-Volmer equation.

$$\frac{I_0}{I_0 - I} = \frac{1}{f_a K_{SV}} \frac{1}{Q} + \frac{1}{f_a}$$

where f_a is the fraction of fluorophore accessible to the quencher and K_{SV} is the modified Stern-Volmer quenching constant.

3.0 ^{1}H and ^{13}C NMR Spectra of compounds

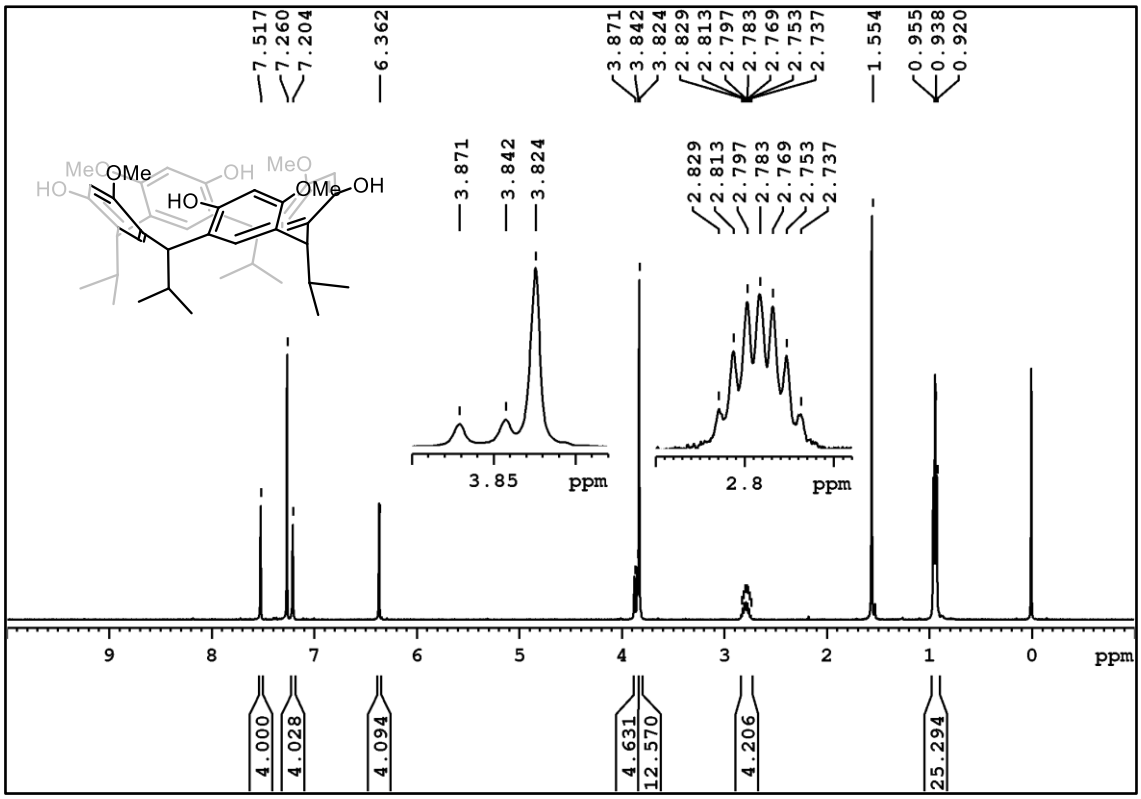

Figure S1: ^{1}H NMR spectrum of **2a** in $CDCl_3$.

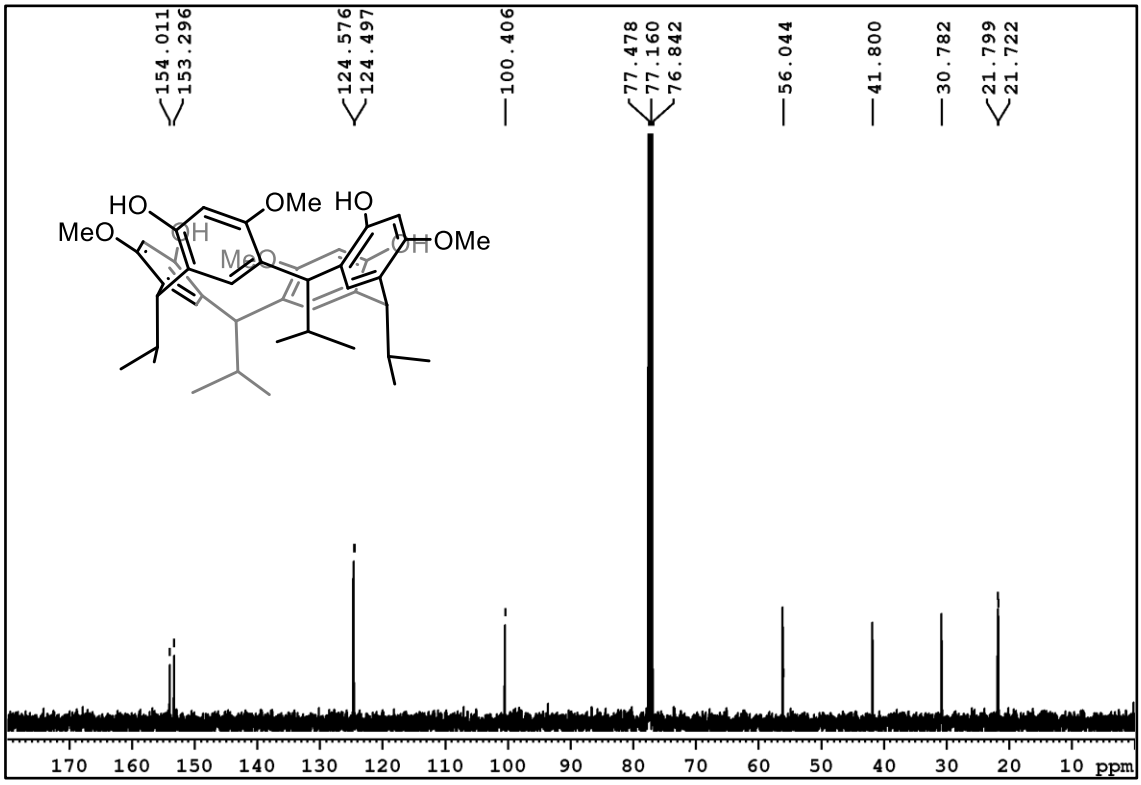

Figure S2: ^{13}C {^{1}H} NMR spectrum of **2b** in $CDCl_3$.

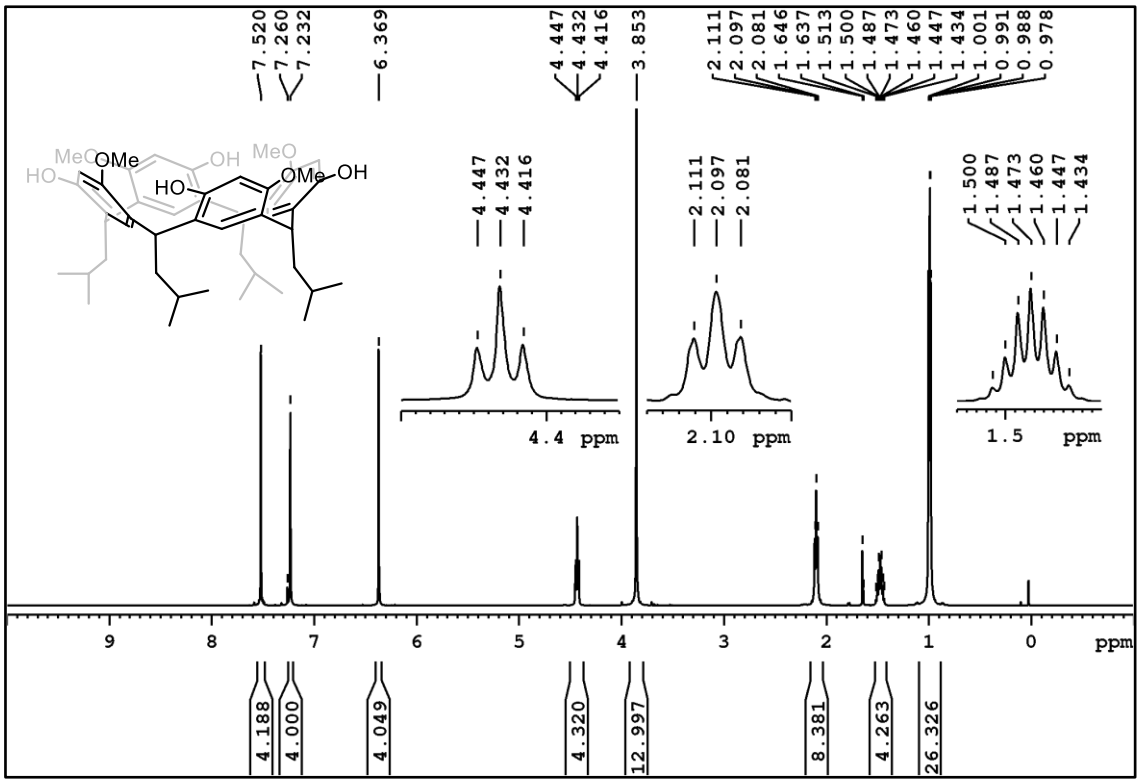

Figure S3: ^{1}H NMR spectrum of **2b** in $CDCl_3$.

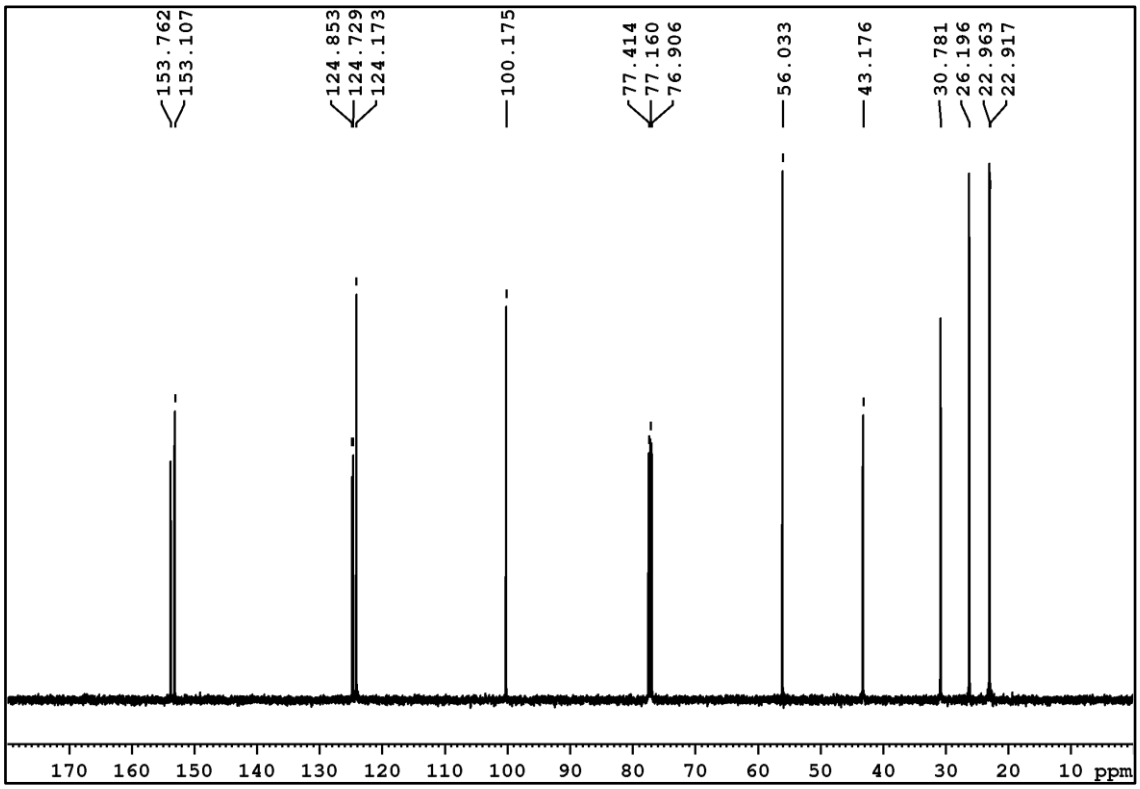

Figure S4: ^{13}C {^{1}H} NMR spectrum of **2b** in $CDCl_3$.

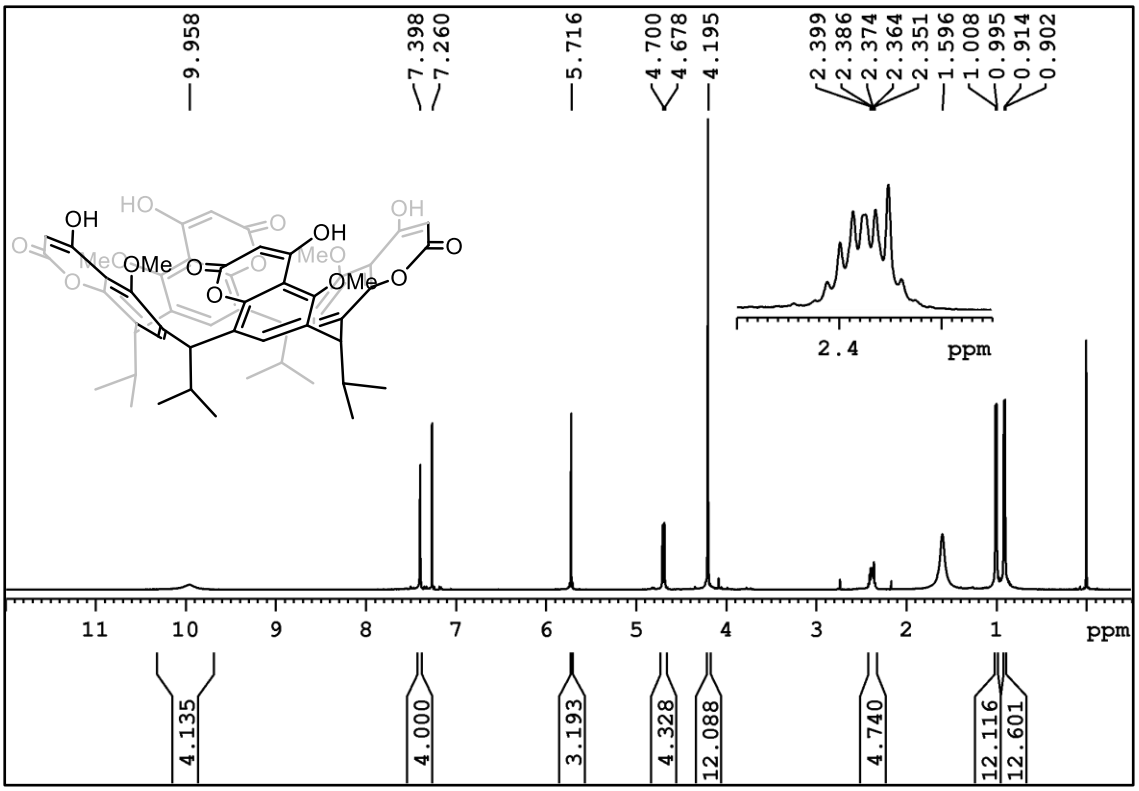

Figure S5: ^{1}H NMR spectrum of **1a** in $CDCl_3$

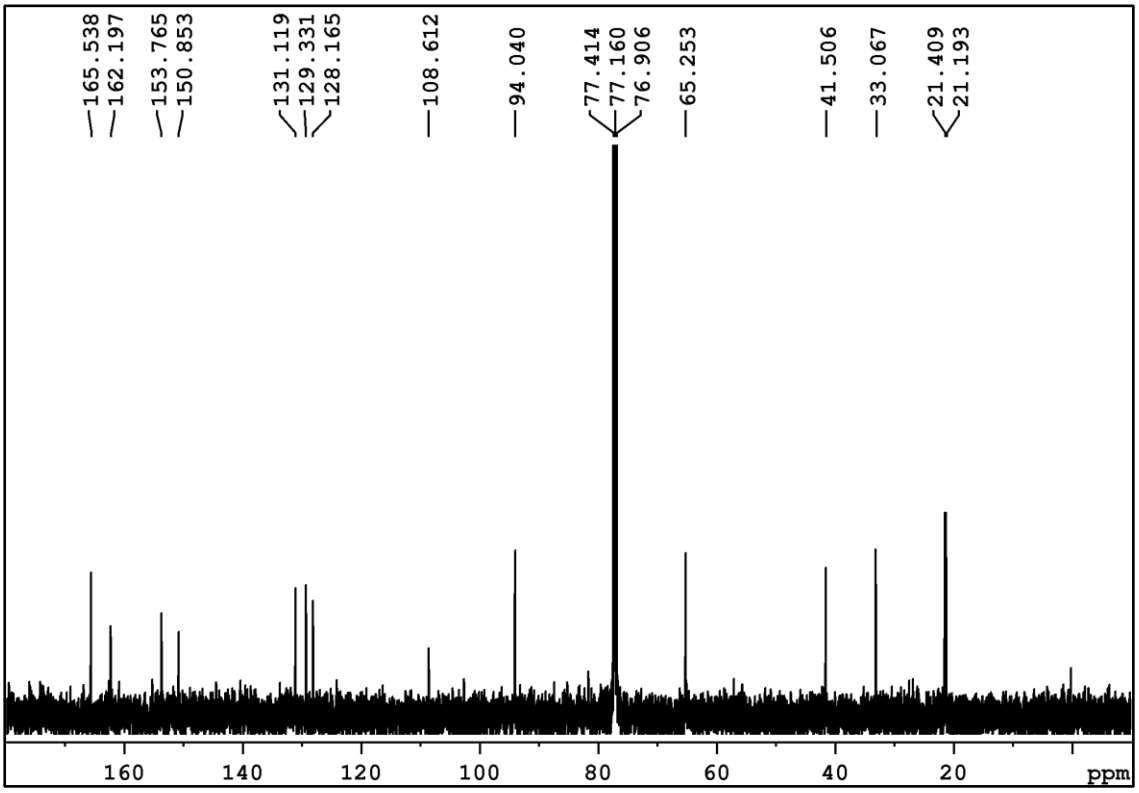

Figure S6: ^{13}C $\{^{1}H\}$ NMR spectrum of **1a** in $CDCl_3$.

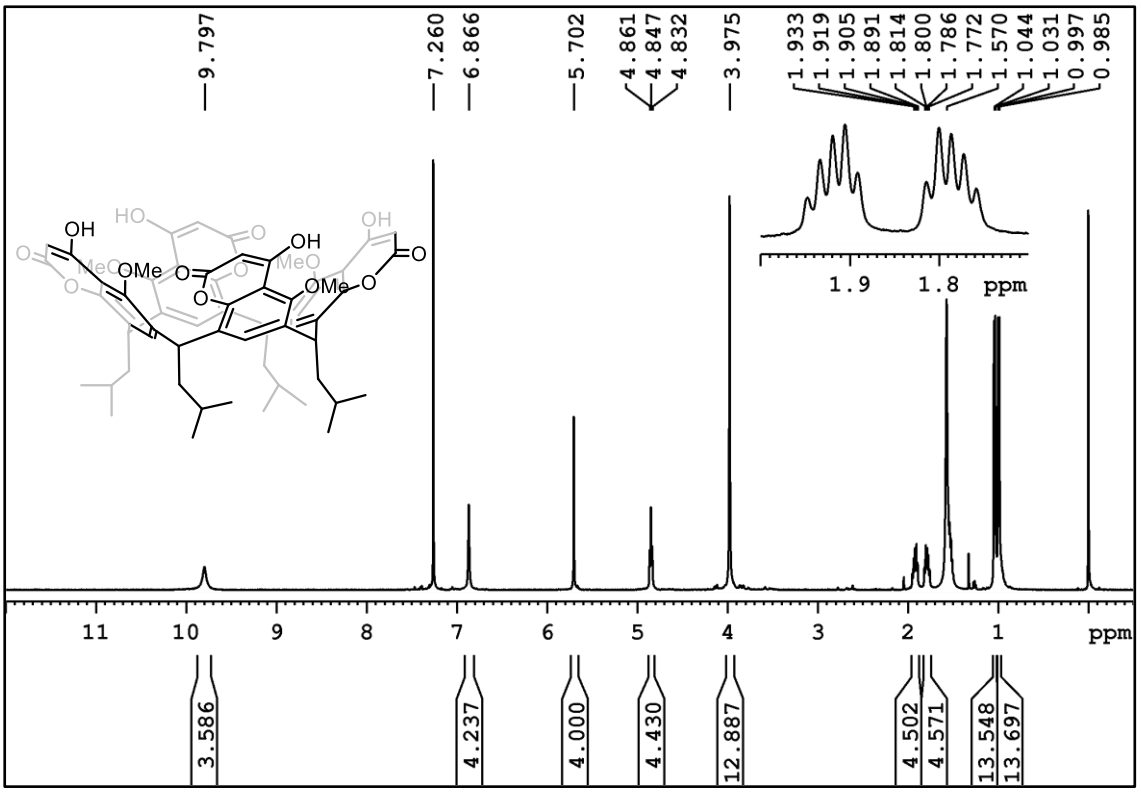

Figure S7: ^{1}H NMR spectrum of **1b** in $CDCl_3$.

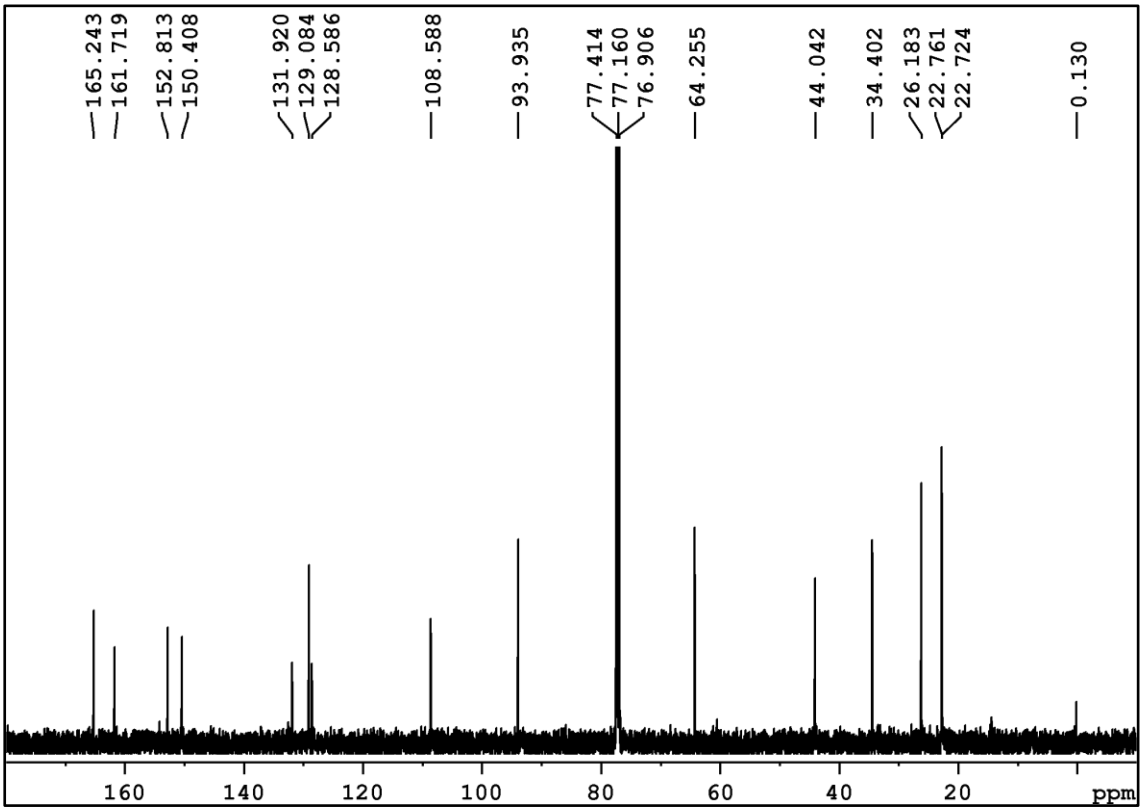

Figure S8: ^{13}C {^{1}H} NMR spectrum of **1b** in $CDCl_3$.

4.0 Absorption and Emission Spectra

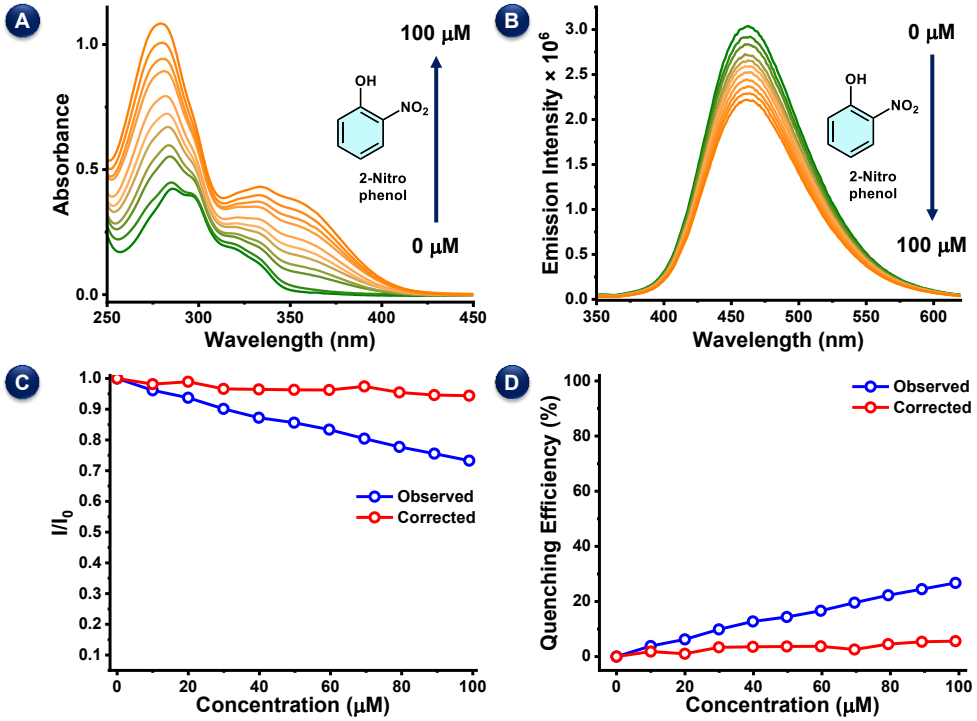

Fig S9: Absorption (A) and emission (λ_{ex} = 320 nm, B) spectral changes, inner filter effect corrected emission intensities (C), and inner filter effect corrected quenching efficiencies (D) of **1a** upon titration against 2-nitrophenol.

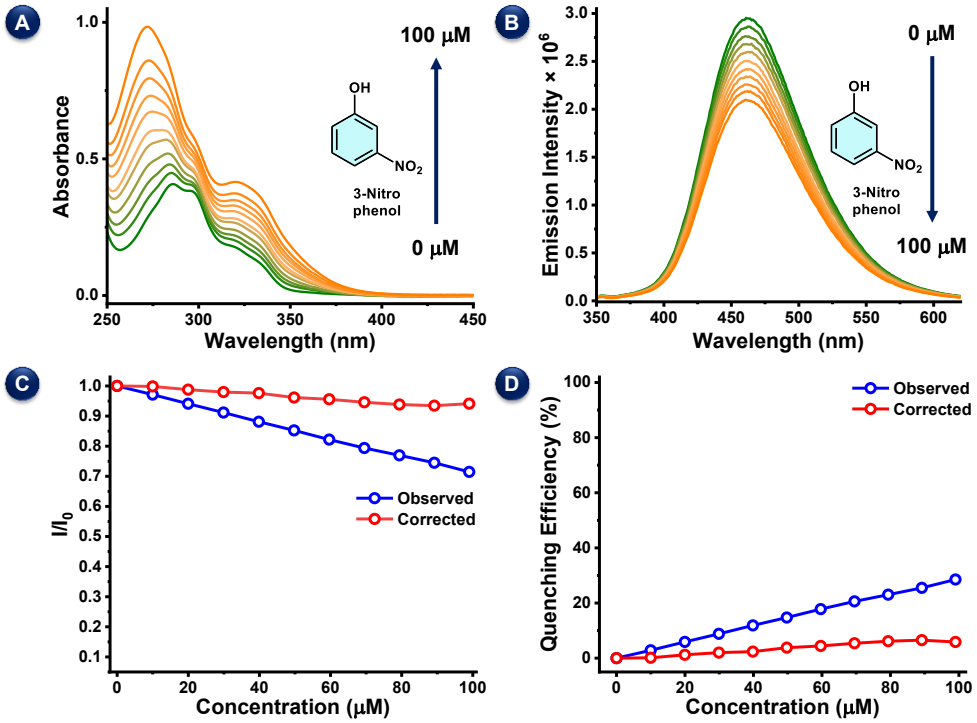

Fig S10: Absorption (A) and emission (λ_{ex} = 320 nm, B) spectral changes, inner filter effect corrected emission intensities (C), and inner filter effect corrected quenching efficiencies (D) of **1a** upon titration against 3-nitrophenol.

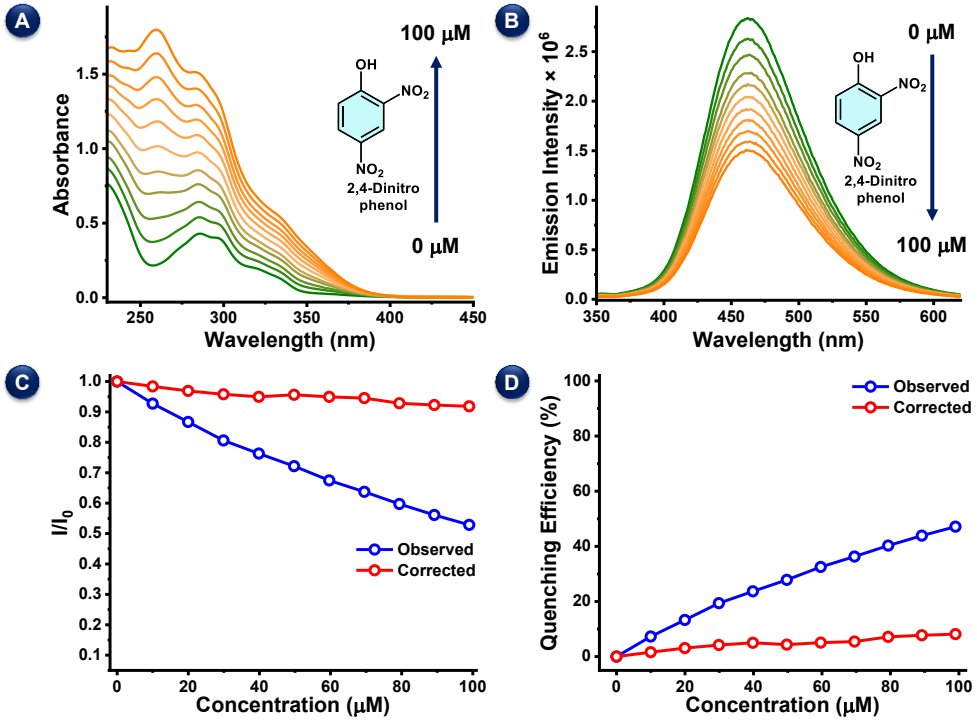

Fig S11: Absorption (A) and emission (λ_{ex} = 320 nm, B) spectral changes, inner filter effect corrected emission intensities (C), and inner filter effect corrected quenching efficiencies (D) of **1a** upon titration against 2,4-dinitrophenol.

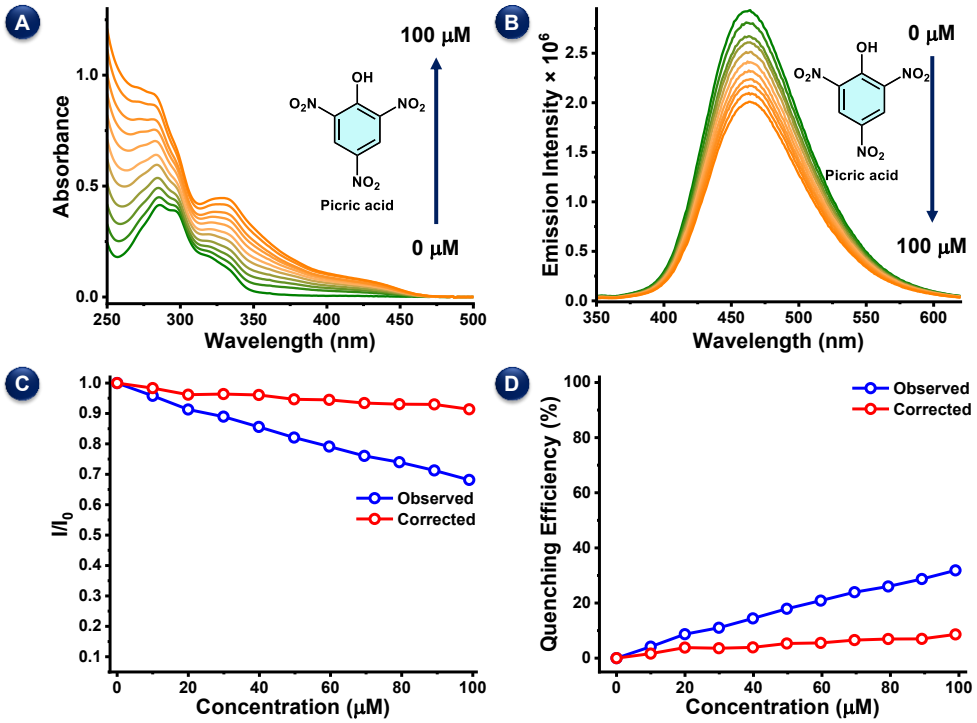

Fig S12: Absorption (A) and emission (λ_{ex} = 320 nm, B) spectral changes, inner filter effect corrected emission intensities (C), and inner filter effect corrected quenching efficiencies (D) of **1a** upon titration against picric acid.

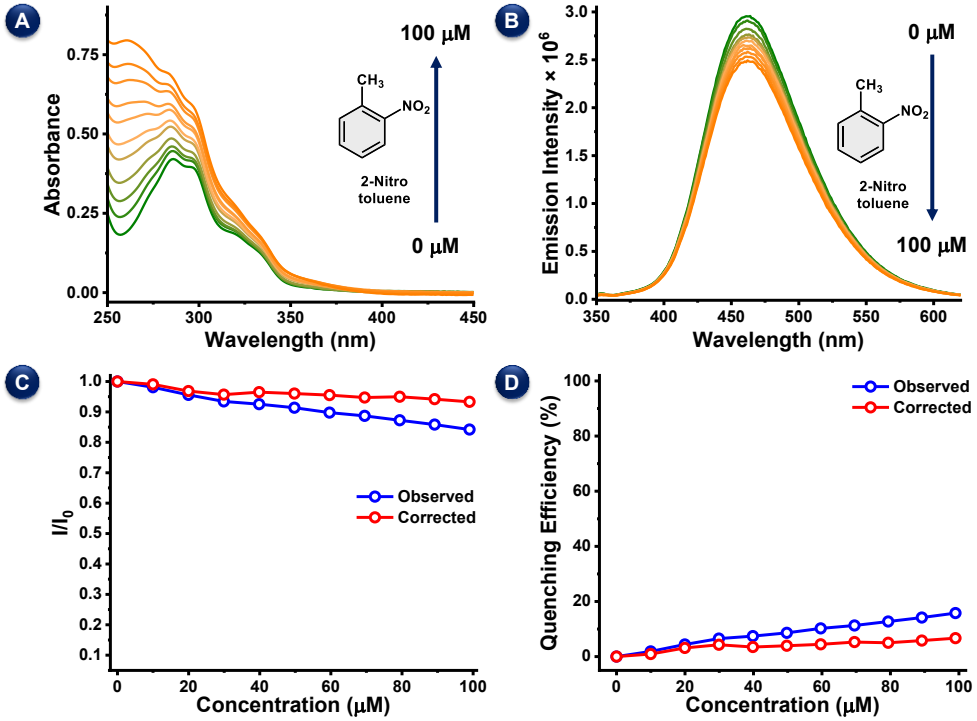

Fig S13: Absorption (A) and emission (λ_{ex} = 320 nm, B) spectral changes, inner filter effect corrected emission intensities (C), and inner filter effect corrected quenching efficiencies (D) of **1a** upon titration against 2-nitrotoluene.

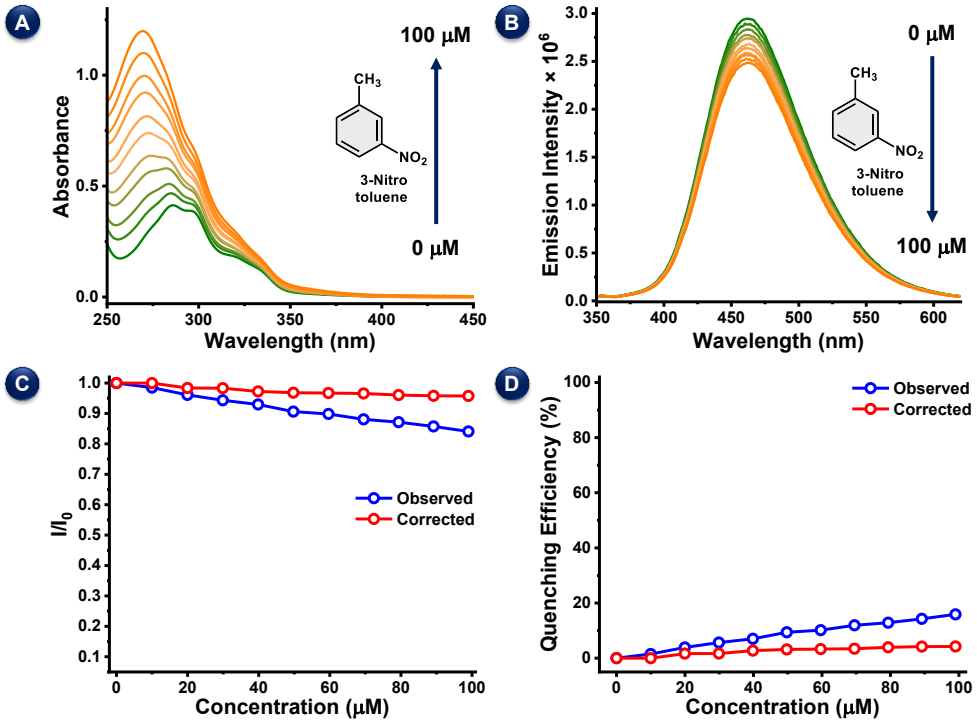

Fig S14: Absorption (A) and emission (λ_{ex} = 320 nm, B) spectral changes, inner filter effect corrected emission intensities (C), and inner filter effect corrected quenching efficiencies (D) of **1a** upon titration against 3-nitrotoluene.

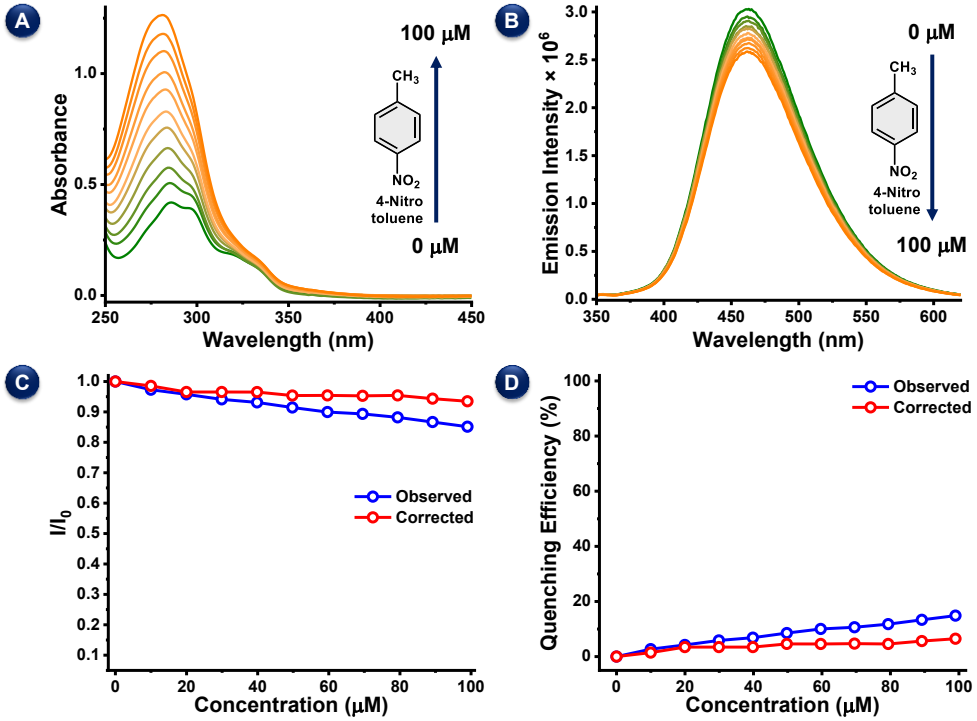

Fig S15: Absorption (A) and emission (λ_{ex} = 320 nm, B) spectral changes, inner filter effect corrected emission intensities (C), and inner filter effect corrected quenching efficiencies (D) of **1a** upon titration against 4-nitrotoluene.

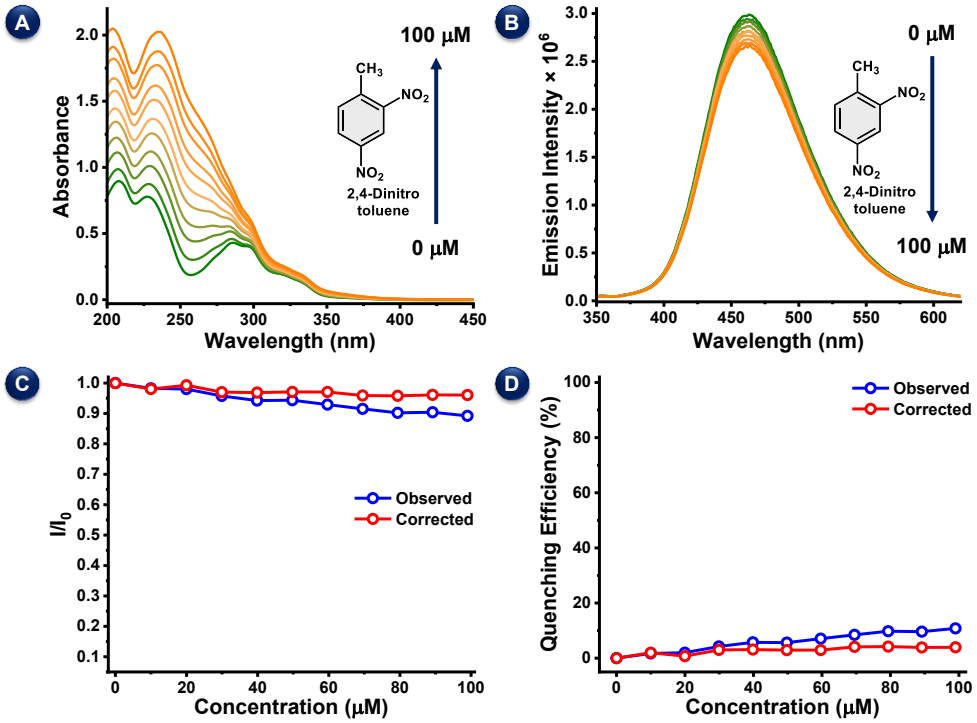

Fig S16: Absorption (A) and emission (λ_{ex} = 320 nm, B) spectral changes, inner filter effect corrected emission intensities (C), and inner filter effect corrected quenching efficiencies (D) of **1a** upon titration against 2,4-dinitrotoluene.

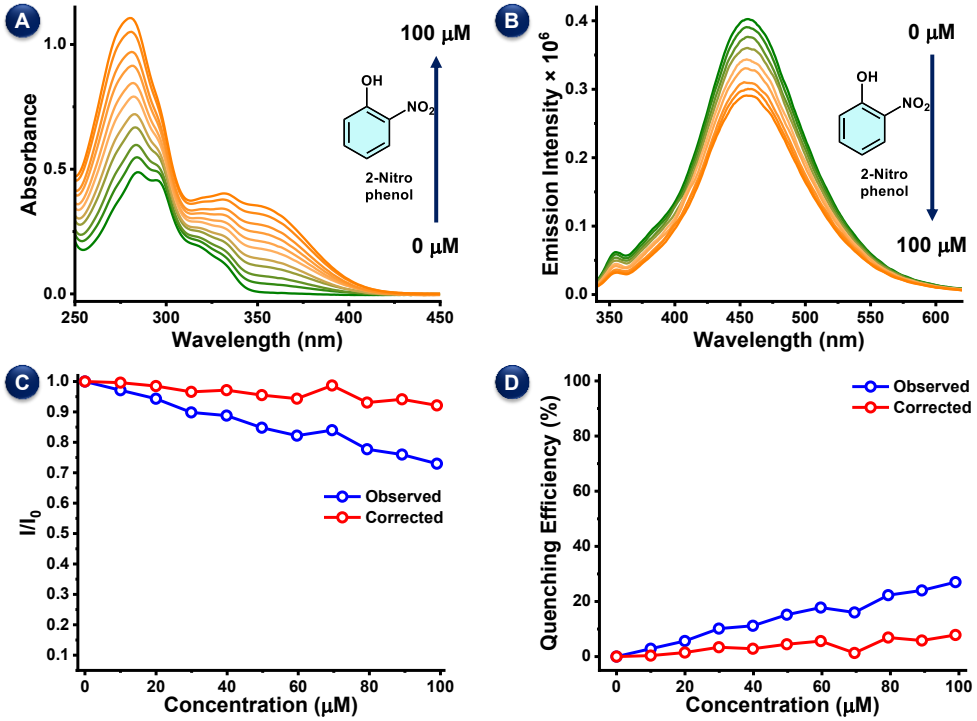

Fig S17: Absorption (A) and emission (λ_{ex} = 320 nm, B) spectral changes, inner filter effect corrected emission intensities (C), and inner filter effect corrected quenching efficiencies (D) of **1b** upon titration against 2-nitrophenol.

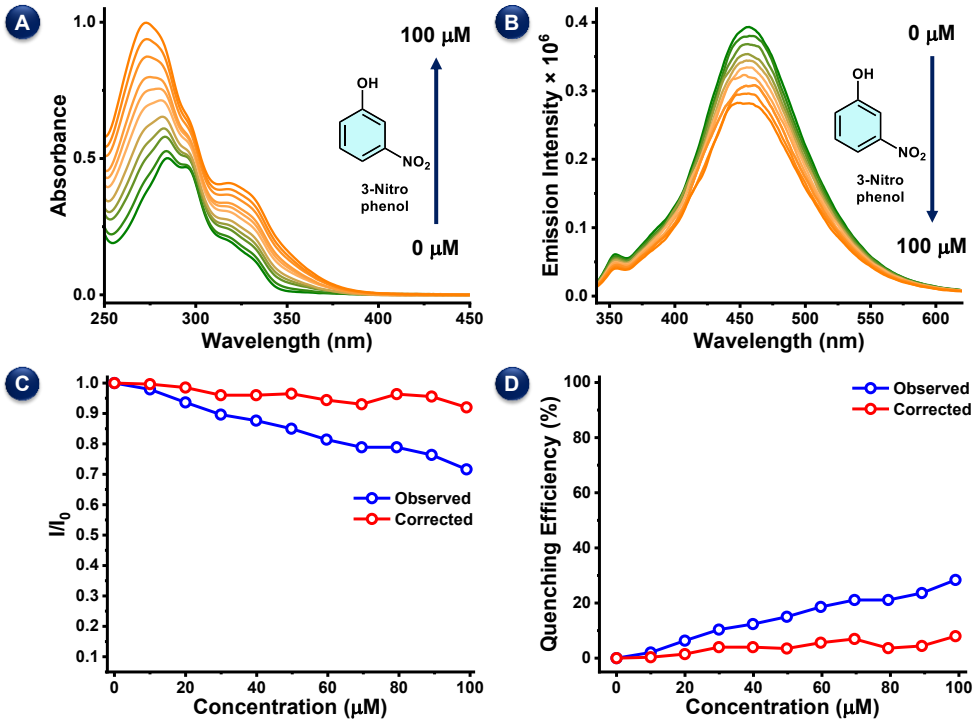

Fig S18: Absorption (A) and emission (λ_{ex} = 320 nm, B) spectral changes, inner filter effect corrected emission intensities (C), and inner filter effect corrected quenching efficiencies (D) of **1b** upon titration against 3-nitrophenol.

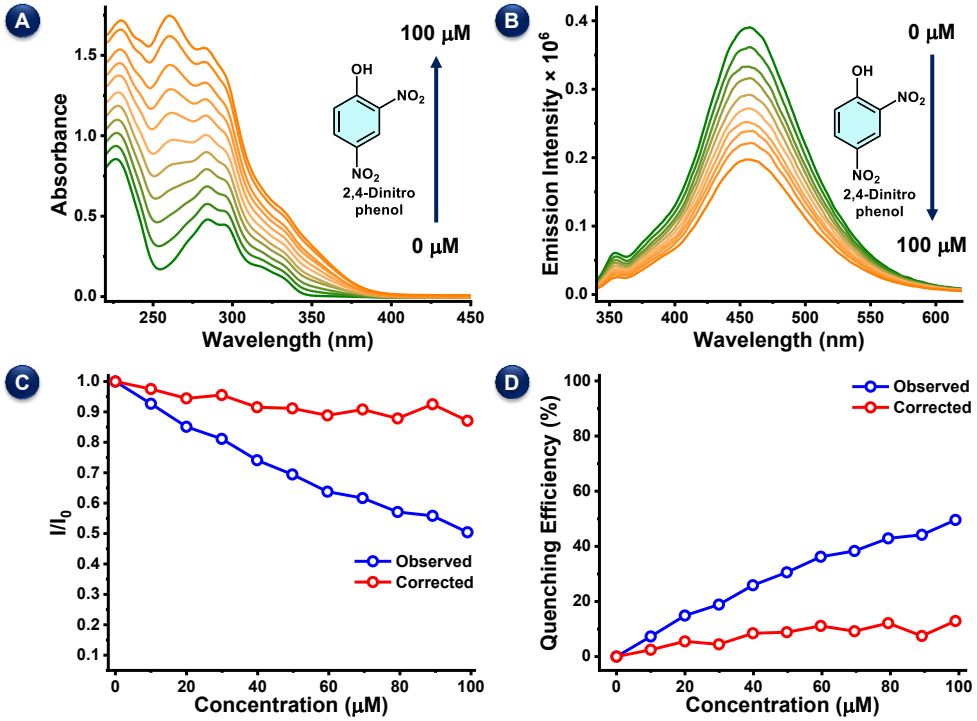

Fig S19: Absorption (A) and emission (λ_{ex} = 320 nm, B) spectral changes, inner filter effect corrected emission intensities (C), and inner filter effect corrected quenching efficiencies (D) of **1b** upon titration against 2,4-dinitrophenol.

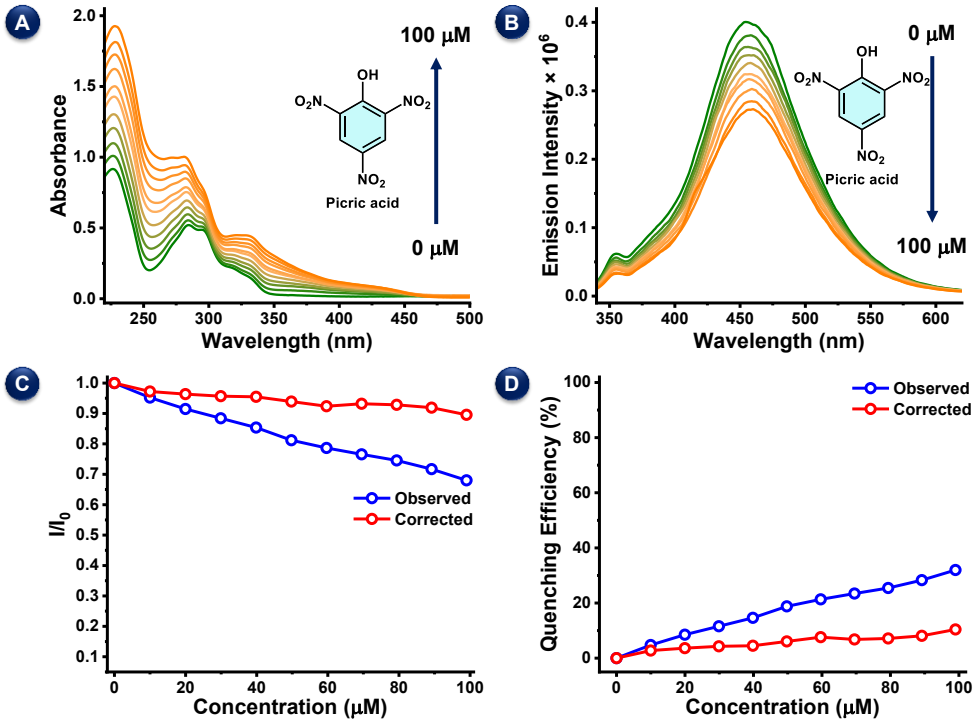

Fig S20: Absorption (A) and emission (λ_{ex} = 320 nm, B) spectral changes, inner filter effect corrected emission intensities (C), and inner filter effect corrected quenching efficiencies (D) of **1b** upon titration against picric acid.

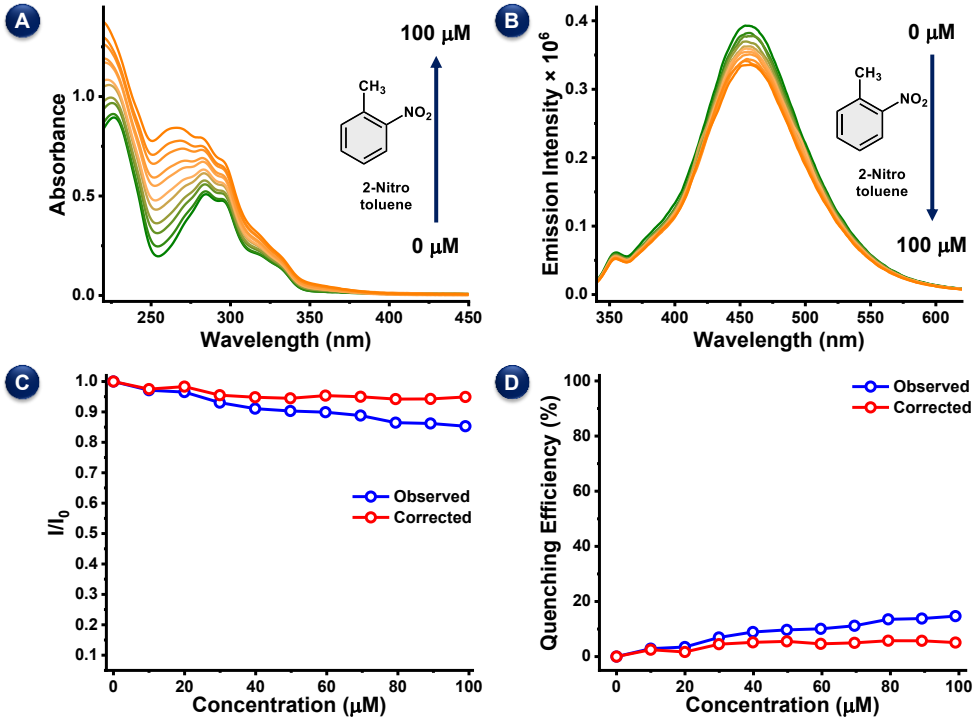

Fig S21: Absorption (A) and emission (λ_{ex} = 320 nm, B) spectral changes, inner filter effect corrected emission intensities (C), and inner filter effect corrected quenching efficiencies (D) of **1b** upon titration against 2-nitrotoluene.

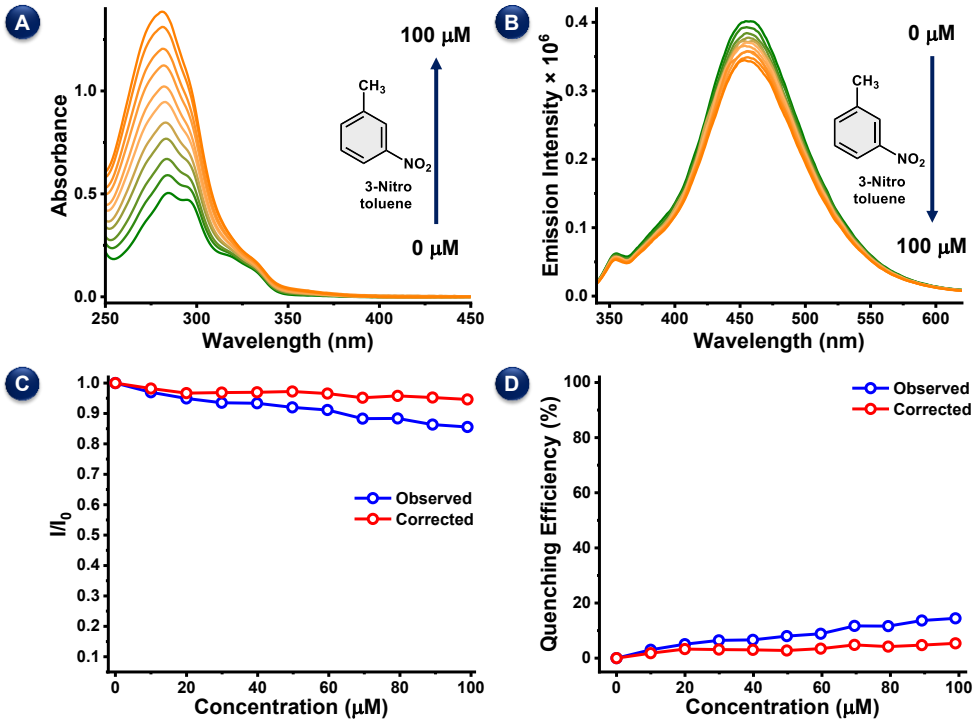

Fig S22: Absorption (A) and emission (λ_{ex} = 320 nm, B) spectral changes, inner filter effect corrected emission intensities (C), and inner filter effect corrected quenching efficiencies (D) of **1b** upon titration against 3-nitrotoluene.

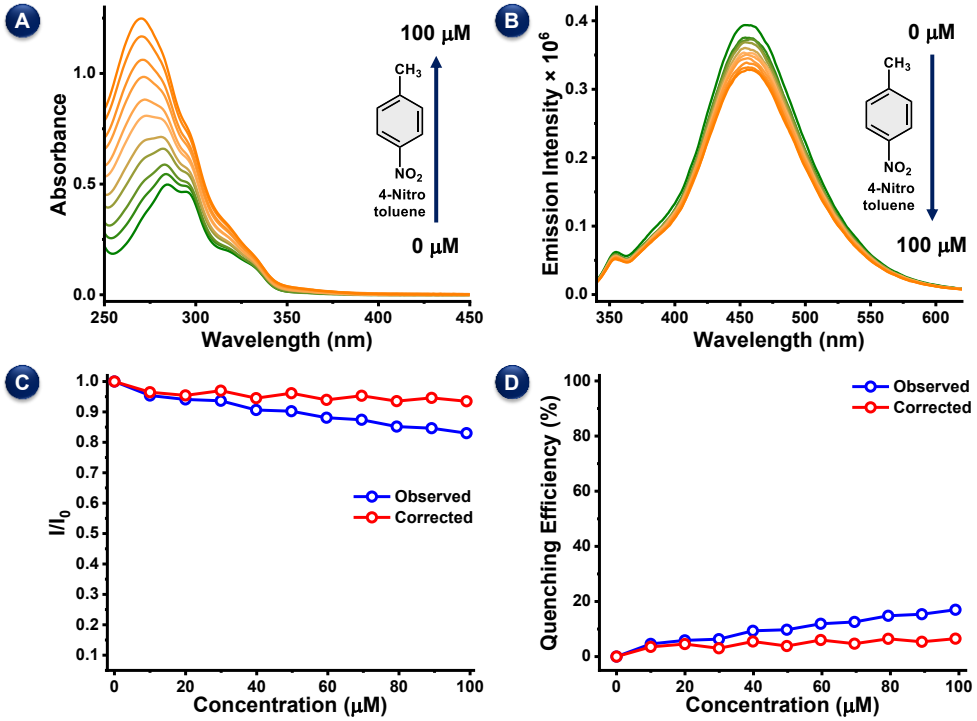

Fig S23: Absorption (A) and emission (λ_{ex} = 320 nm, B) spectral changes, inner filter effect corrected emission intensities (C), and inner filter effect corrected quenching efficiencies (D) of **1b** upon titration against 4-nitrotoluene.

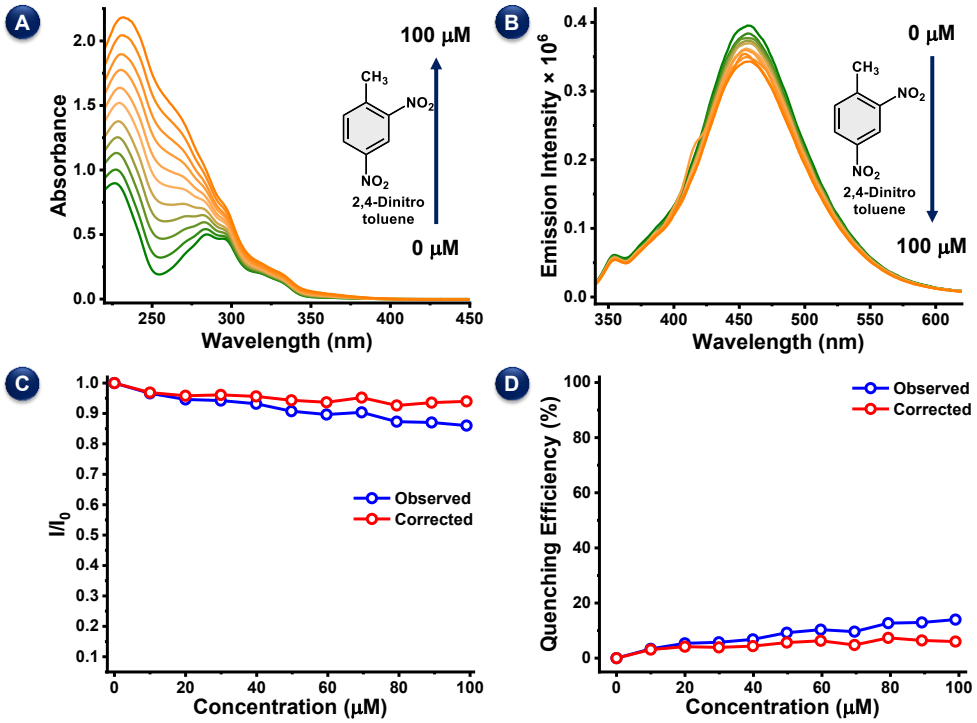

Fig S24: Absorption (A) and emission (λ_{ex} = 320 nm, B) spectral changes, inner filter effect corrected emission intensities (C), and inner filter effect corrected quenching efficiencies (D) of **1b** upon titration against 2,4-dinitrotoluene.

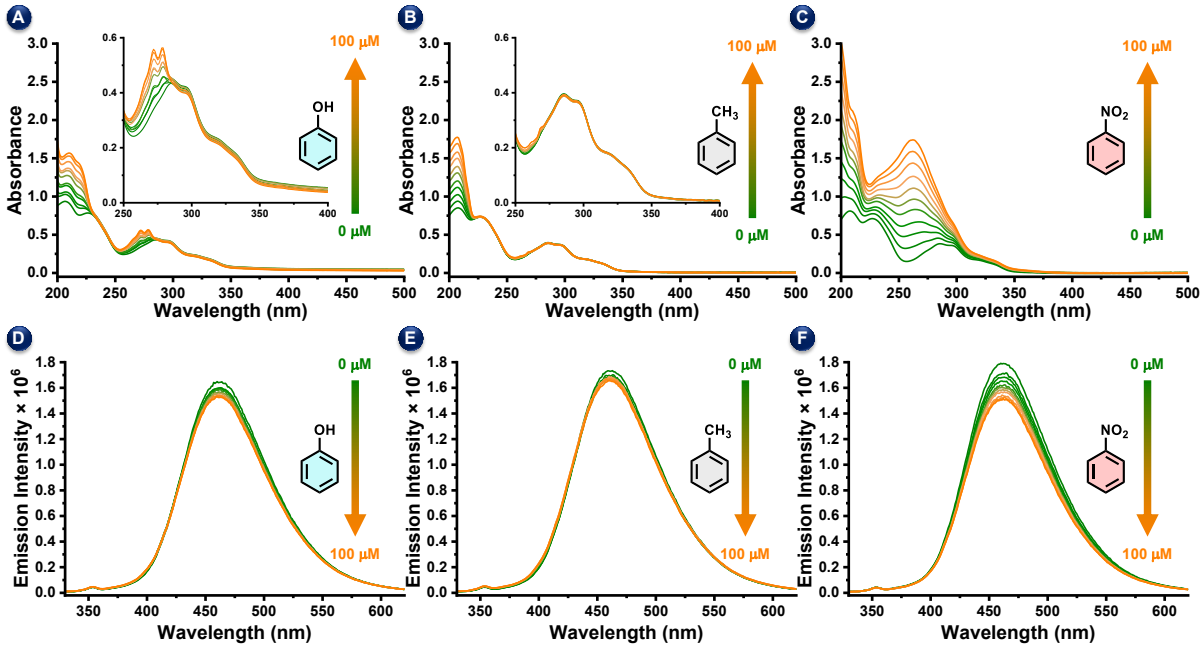

Figure S25: Absorption titration experiments of **1a** vs phenol (A), toluene (B), and nitrobenzene (C). Fluorescence (λ_{ex} = 320 nm) titration experiments of **1a** vs phenol (D), toluene (E), and nitrobenzene (F).

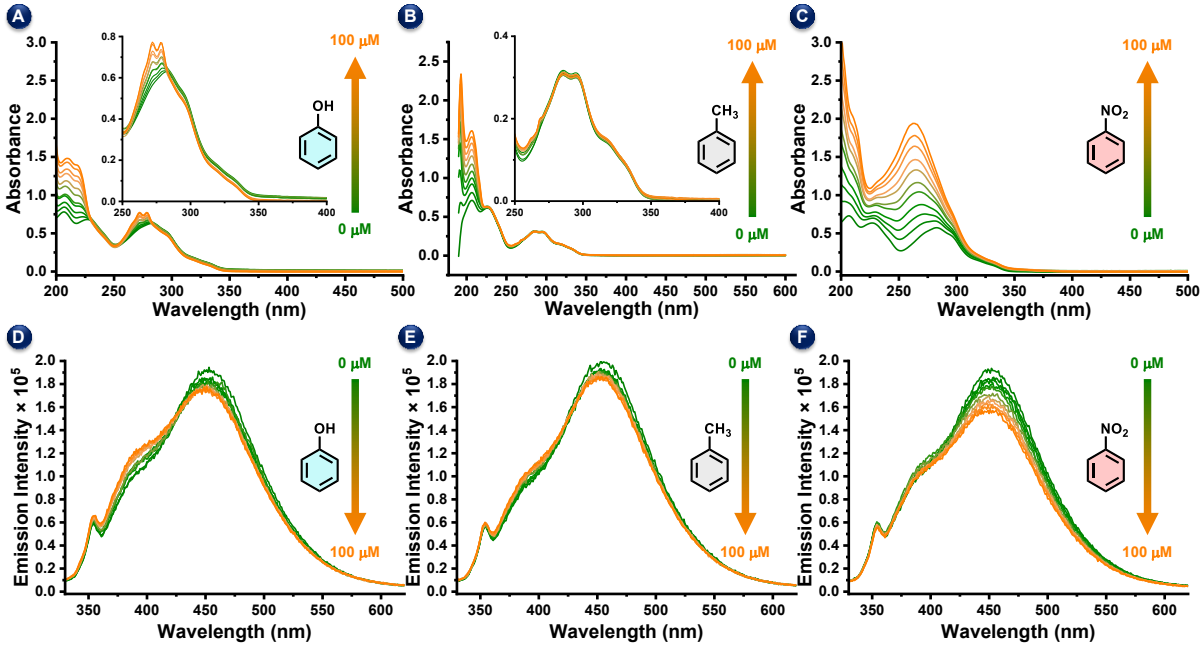

Figure S26: Absorption titration experiments of **1b** vs phenol (A), toluene (B), and nitrobenzene (C). Fluorescence (λ_{ex} = 320 nm) titration experiments of **1b** vs phenol (D), toluene (E), and nitrobenzene (F).

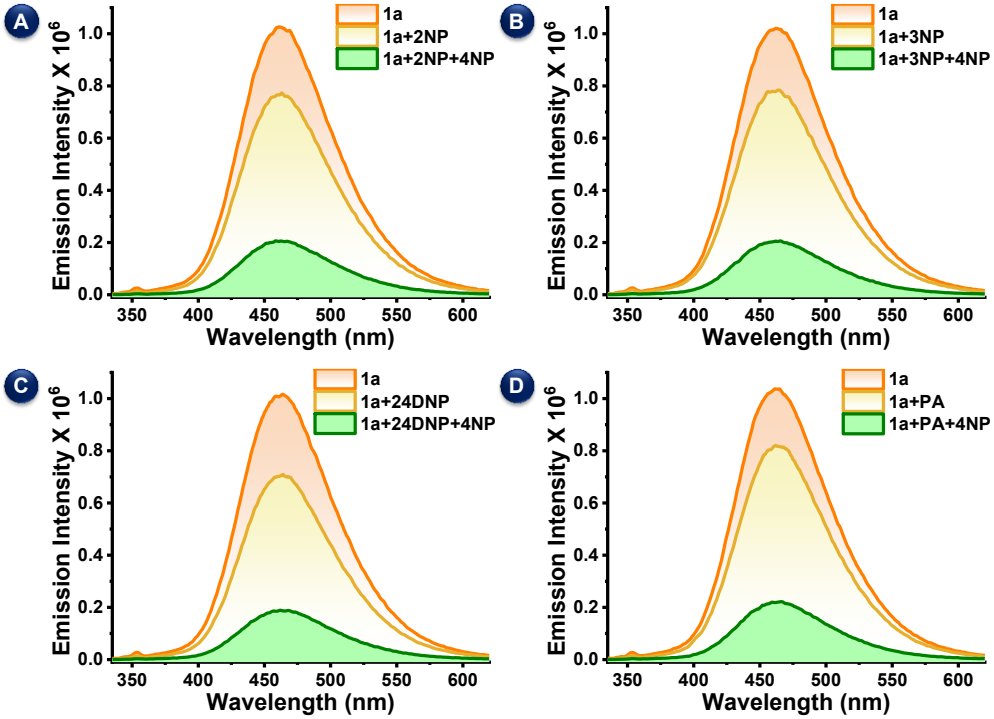

Fig S27: Emission (λ_{ex} = 320 nm) spectral changes during competitive experiment of **1a** with 2-nitrophenol (A), 3-nitrophenol (B), 2,4 dinitrophenol (C), and picric acid (D).

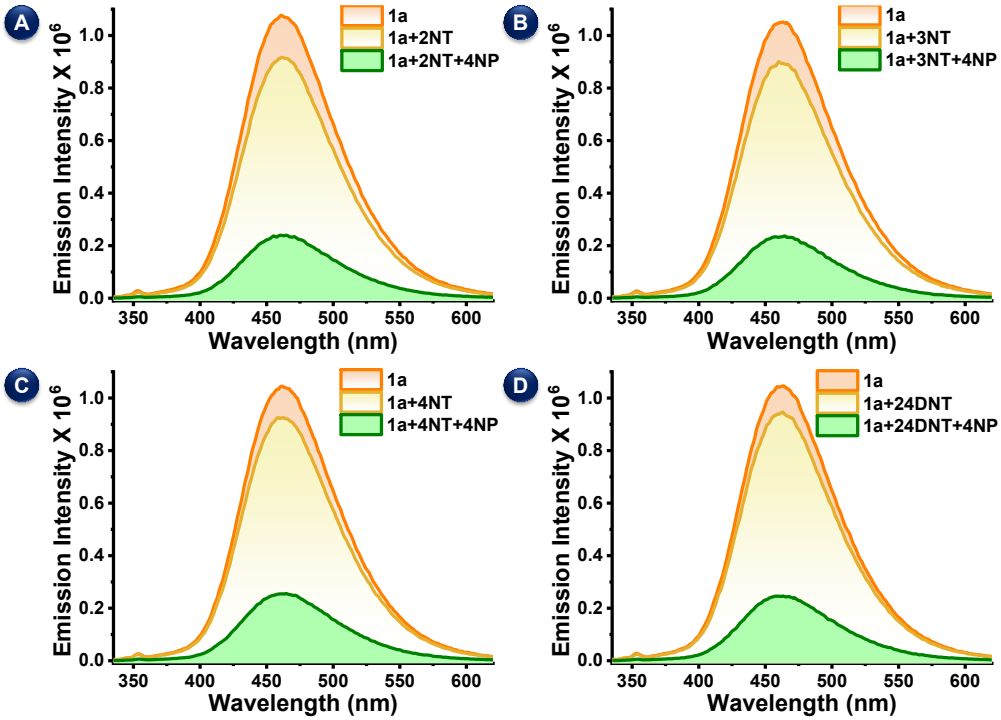

Fig S28: Emission (λ_{ex} = 320 nm) spectral changes during competitive experiment of **1a** with 2-nitrotoluene (A), 3-nitrotoluene (B), 3-nitrotoluene (C), and 2,4-dinitrophenol (D).

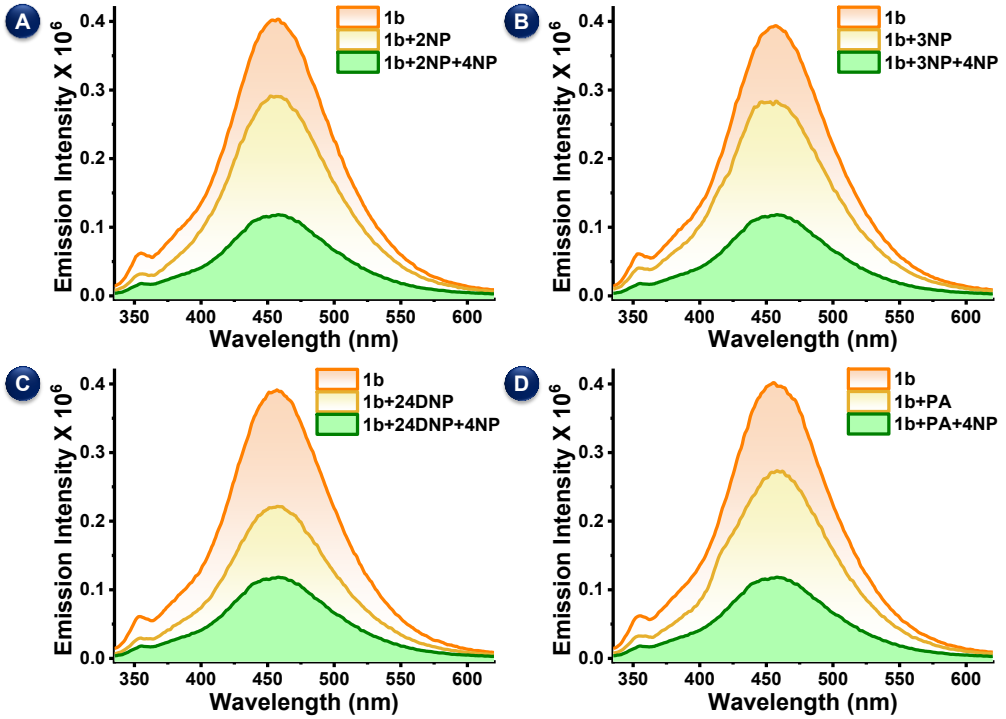

Fig S29: Emission (λ_{ex} = 320 nm) spectral changes during competitive experiments of **1b** with 2-nitrophenol (A), 3-nitrophenol (B), 2,4-dinitrophenol (C), and picric acid (D).

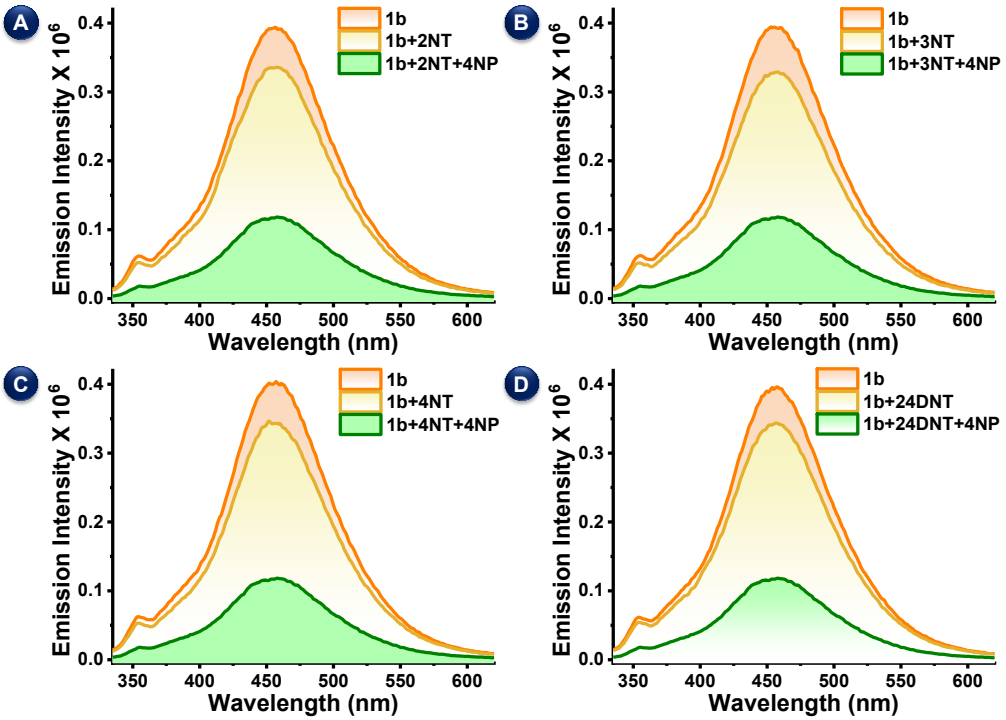

Fig S30: Emission (λ_{ex} = 320 nm) spectral changes during competitive experiments of **1b** with 2-nitrotoluene (A), 3-nitrotoluene (B), 3-nitrotoluene (C), and 2,4-dinitrophenol (D).

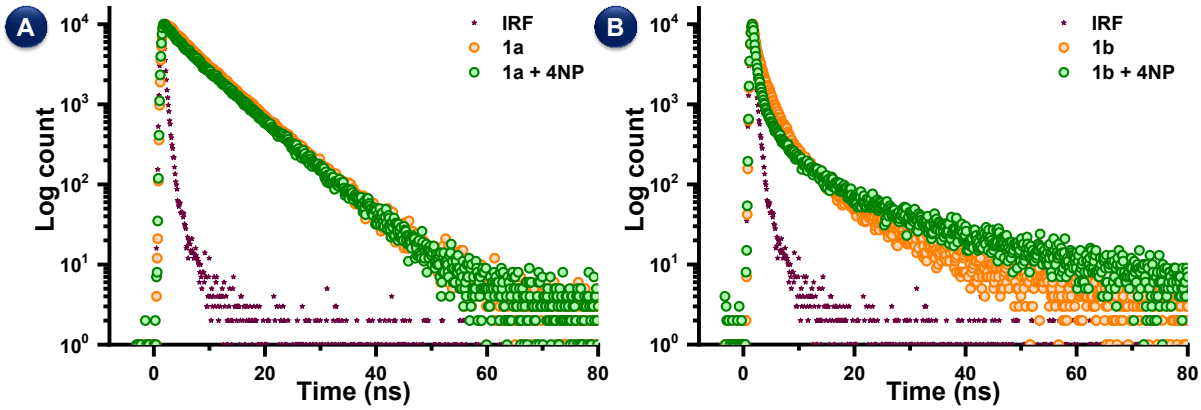

Fig S31: Lifetime measurements of **1a** (A) and **1b** (B) with (blue) and without (red) 4NP.

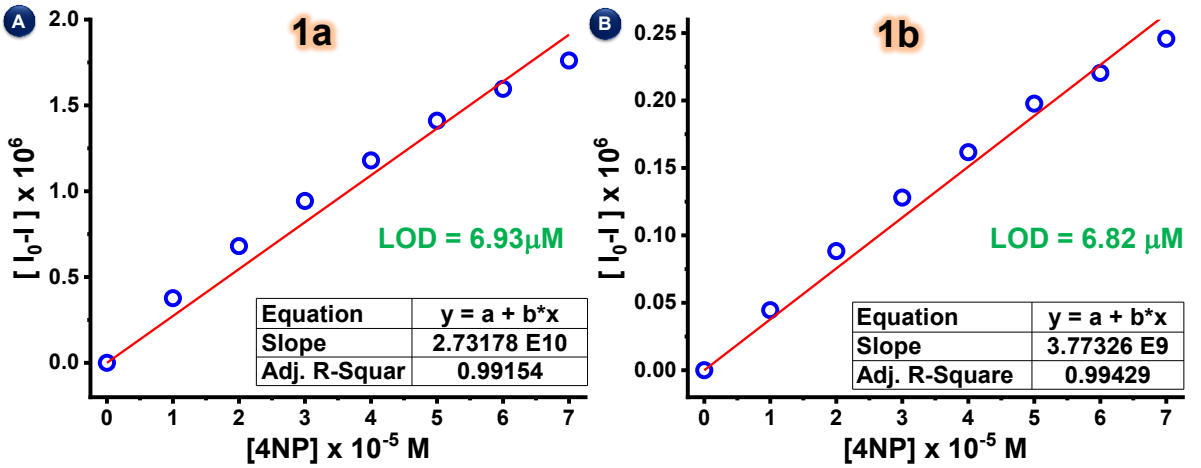

Fig S32: Plot of fluorescence intensity changes vs 4NP concentrations for determining LOD; **1a** (A) and **1b** (B).

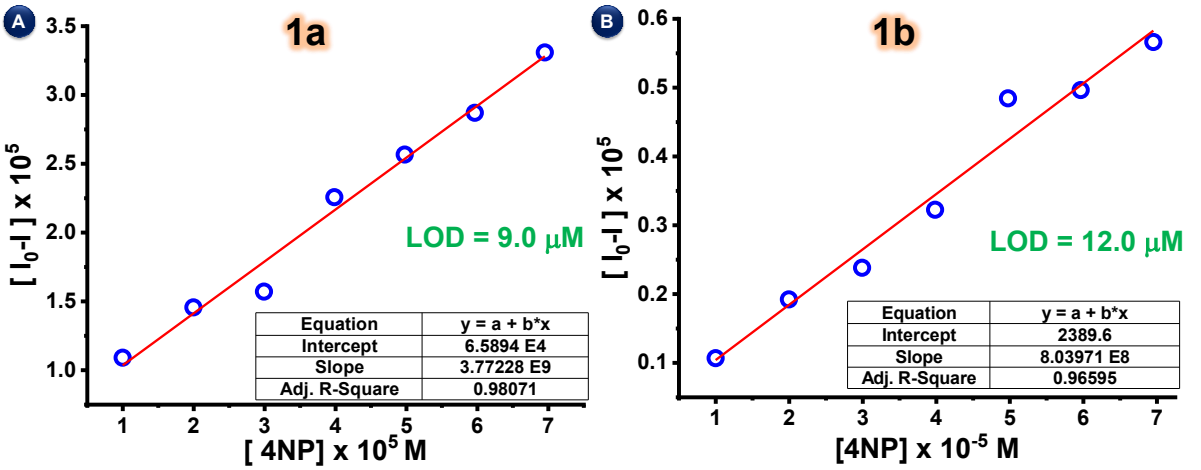

Fig S33: Plot of IFE corrected fluorescence intensity changes vs 4NP concentrations for determining LOD; **1a** (A) and **1b** (B).

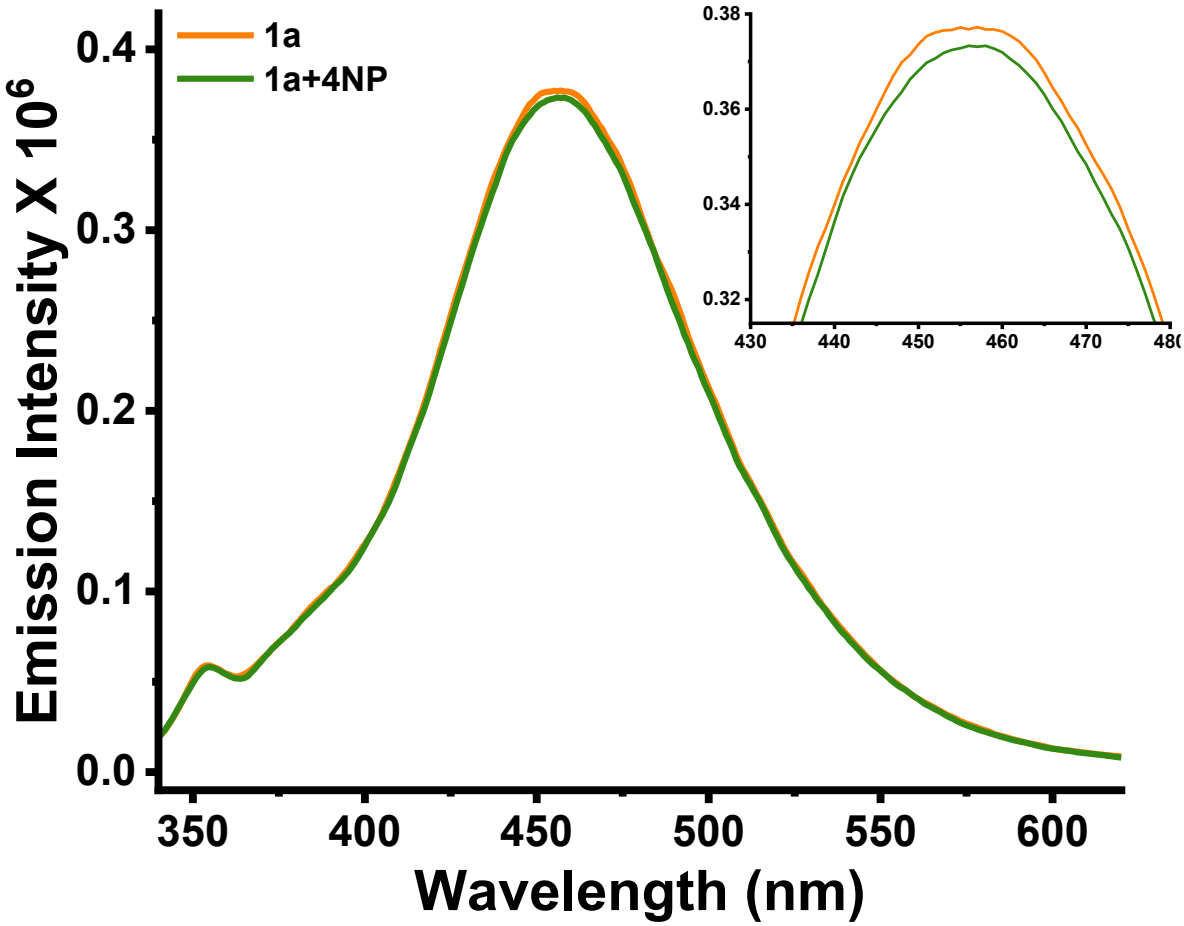

Fig S34: Fluorescence (λ_{ex} = 320 nm) emission intensity changes of **1a** (1×10^{-6} M) detectable at the lowest concentration of 4NP (1×10^{-9} M).

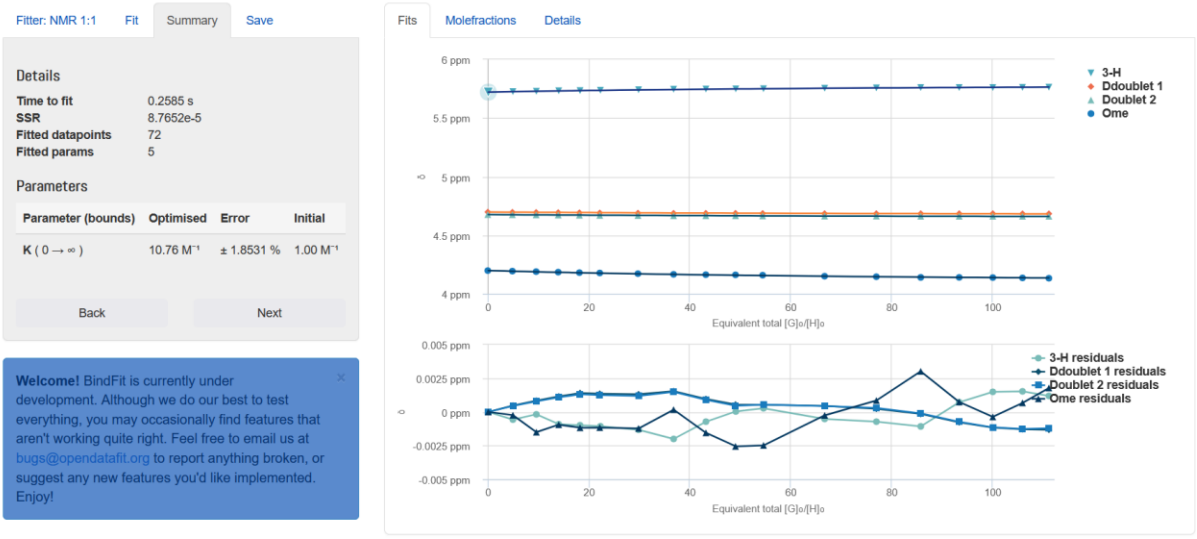

Fig S35: Screenshot of bind-fit plot of chemical shift changes in ^{1}H NMR titration between **1a** and 4NP obtained from the supramolecular.org website.

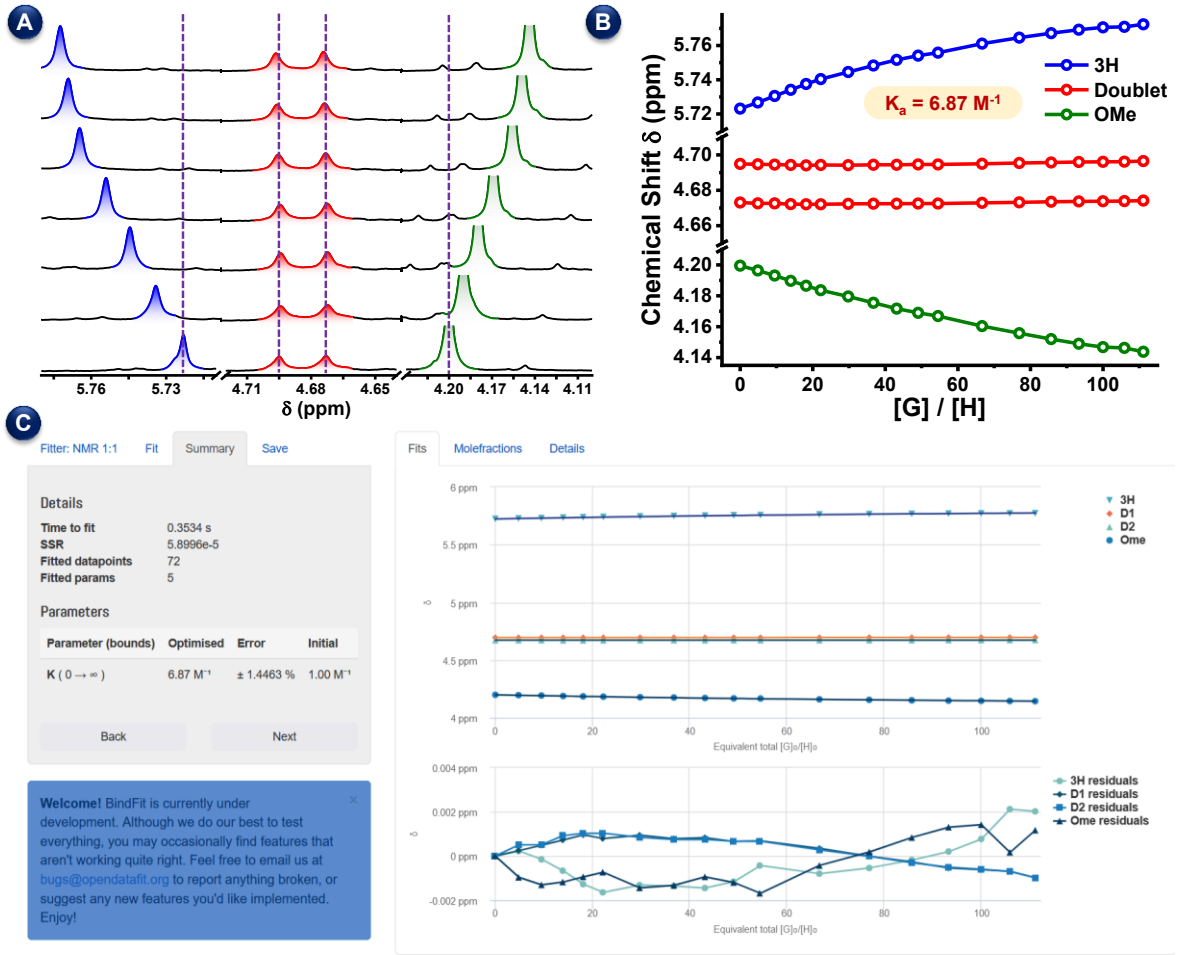

Fig S36: Partial ^{1}H NMR spectrum indicating ^{1}H NMR chemical shift changes of **1a** upon gradual addition of 3NP (A), bind-fit plot of the chemical shift value changes of **1a** versus equivalence of 3NP (B), and screenshot of the bind-fit plot obtained from the supramolecular.org website (C).

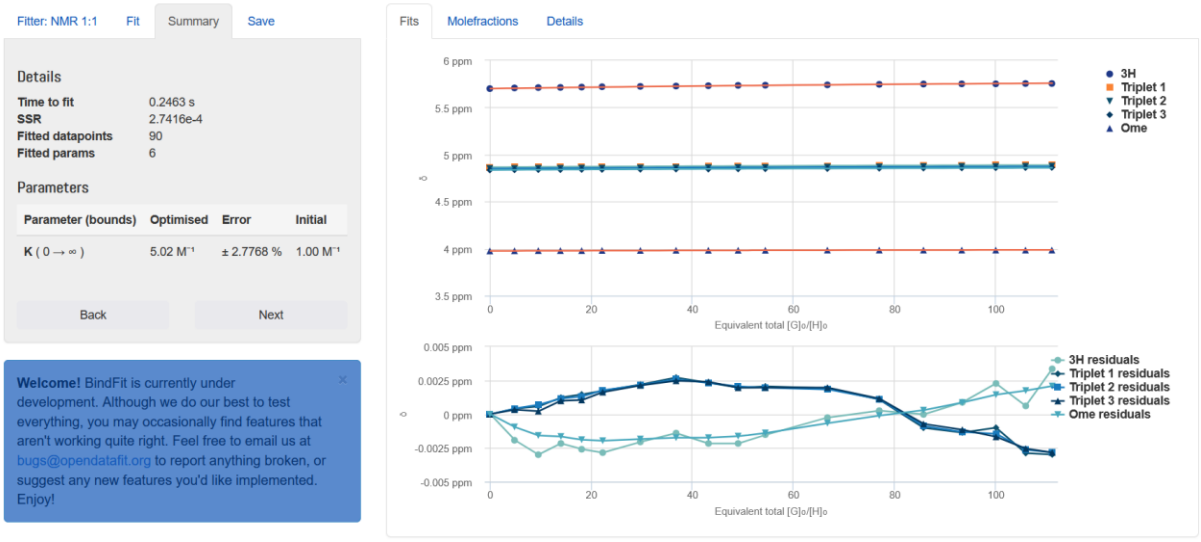

Fig S37: Screenshot of the bind-fit plot of chemical shift changes in ^{1}H NMR titration between **1b** and **4NP** obtained from the supramolecular.org website.

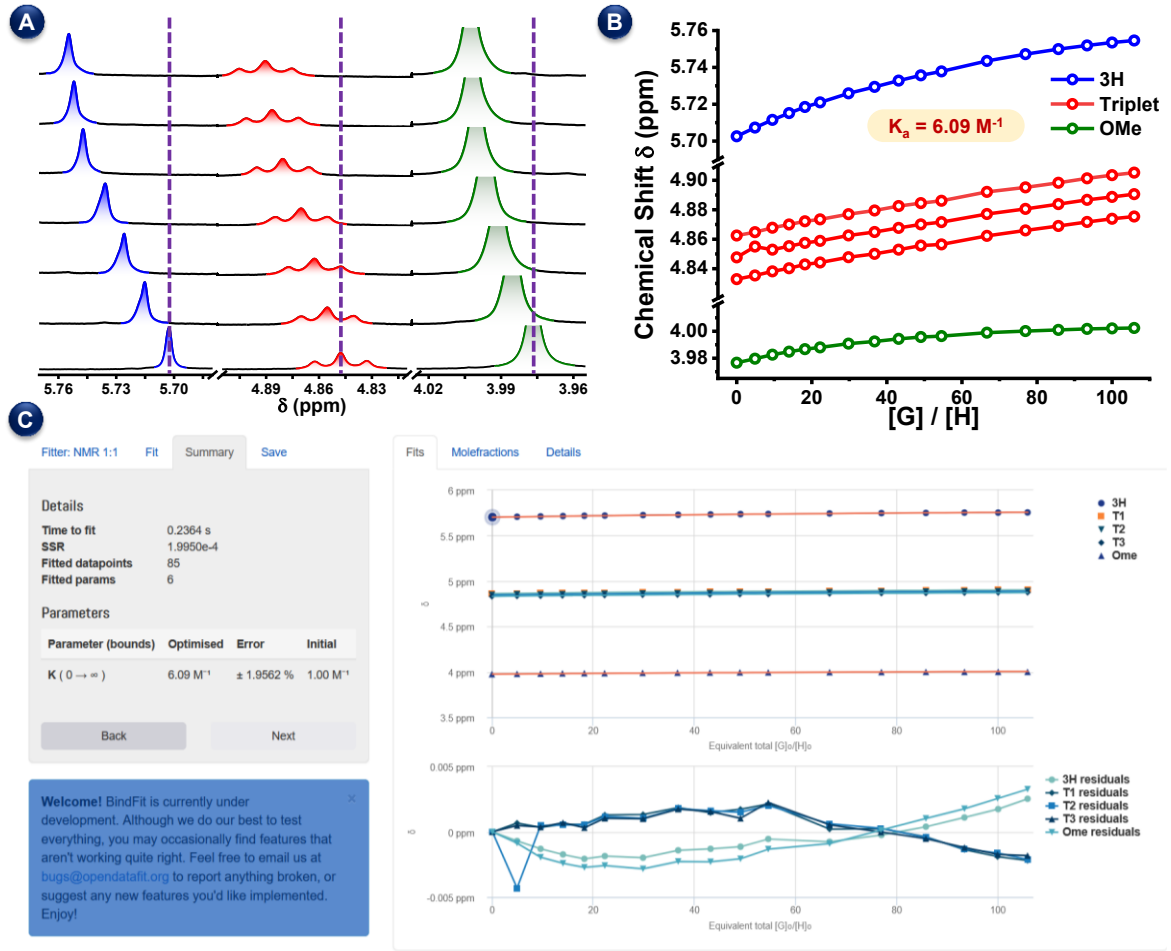

Fig S38: Partial ^{1}H NMR spectrum indicating ^{1}H NMR chemical shift changes of **1b** upon gradual addition of 3NP (A), bind-fit plot of the chemical shift value changes of **1b** versus equivalence of 3NP (B), and screenshot of the bind-fit plot obtained from the supramolecular.org website (C).

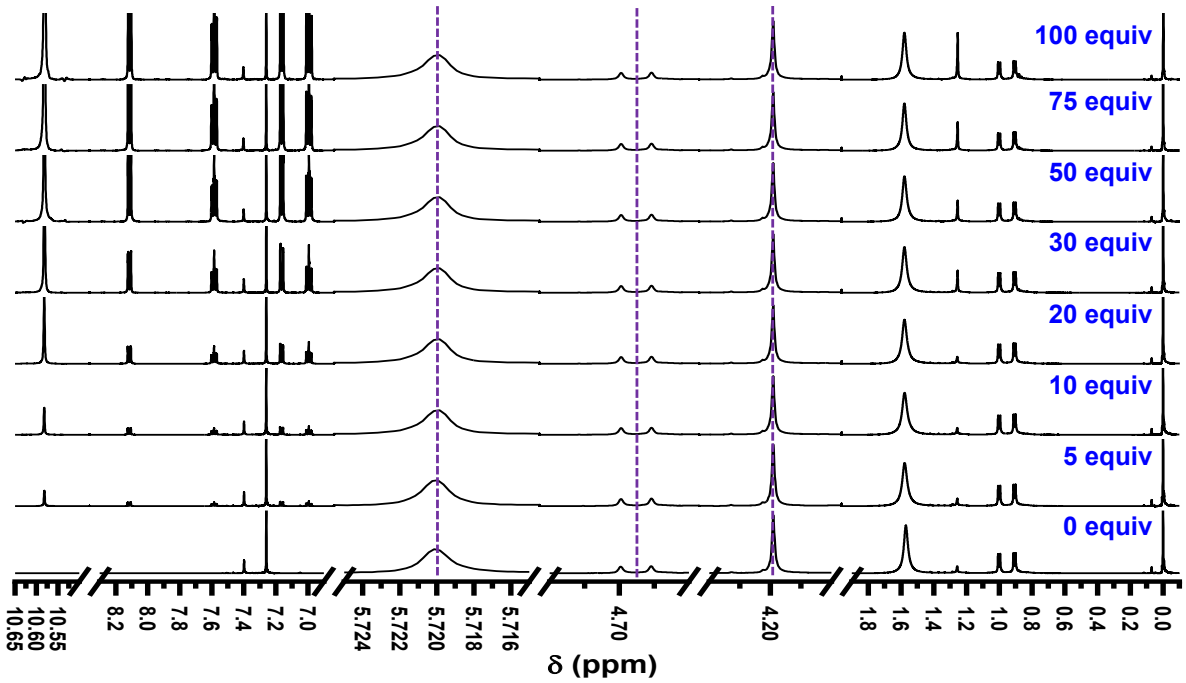

Fig S39: ^{1}H NMR titration results of **1a** against 2-nitrophenol (0 – 100 equiv.).

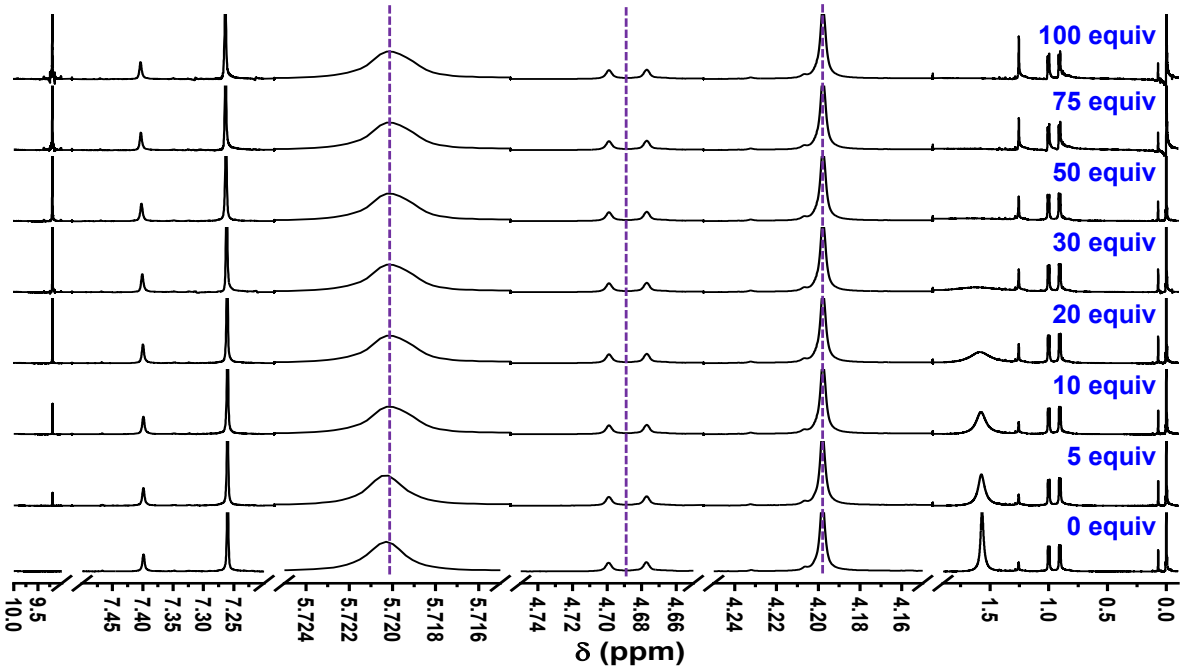

Fig S40: ^{1}H NMR titration results of **1a** against picric acid (0 – 100 equiv.).

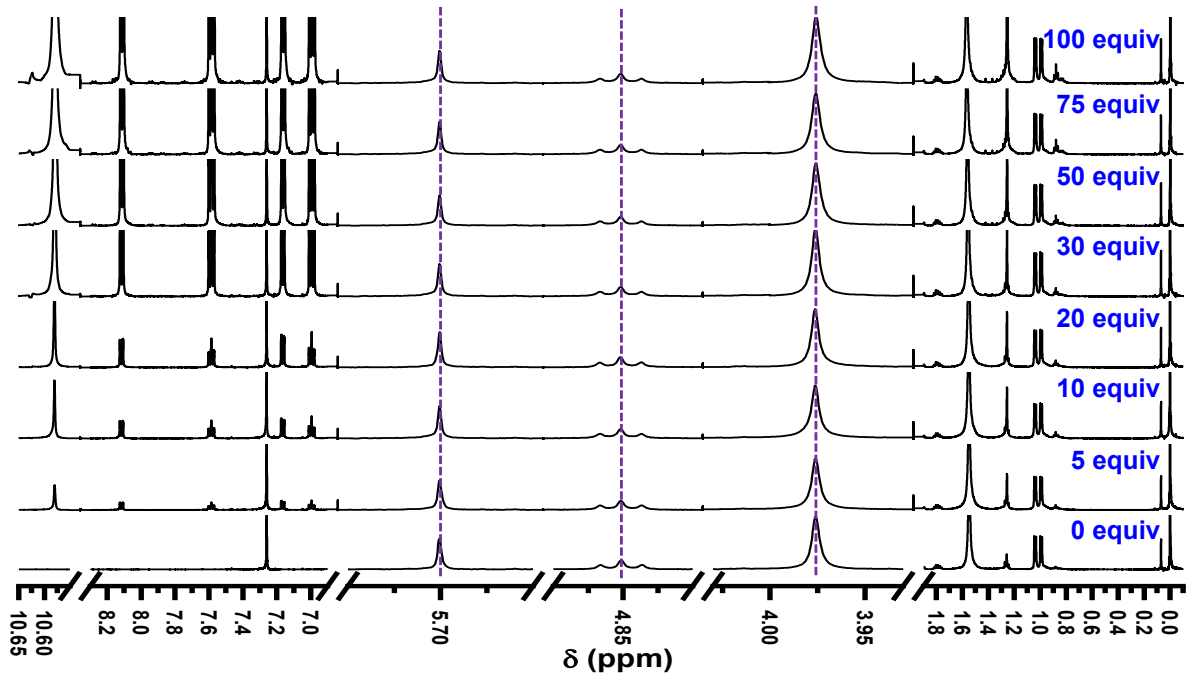

Fig S41: ^{1}H NMR titration results of **1b** against 2-nitrophenol (0 – 100 equiv.).

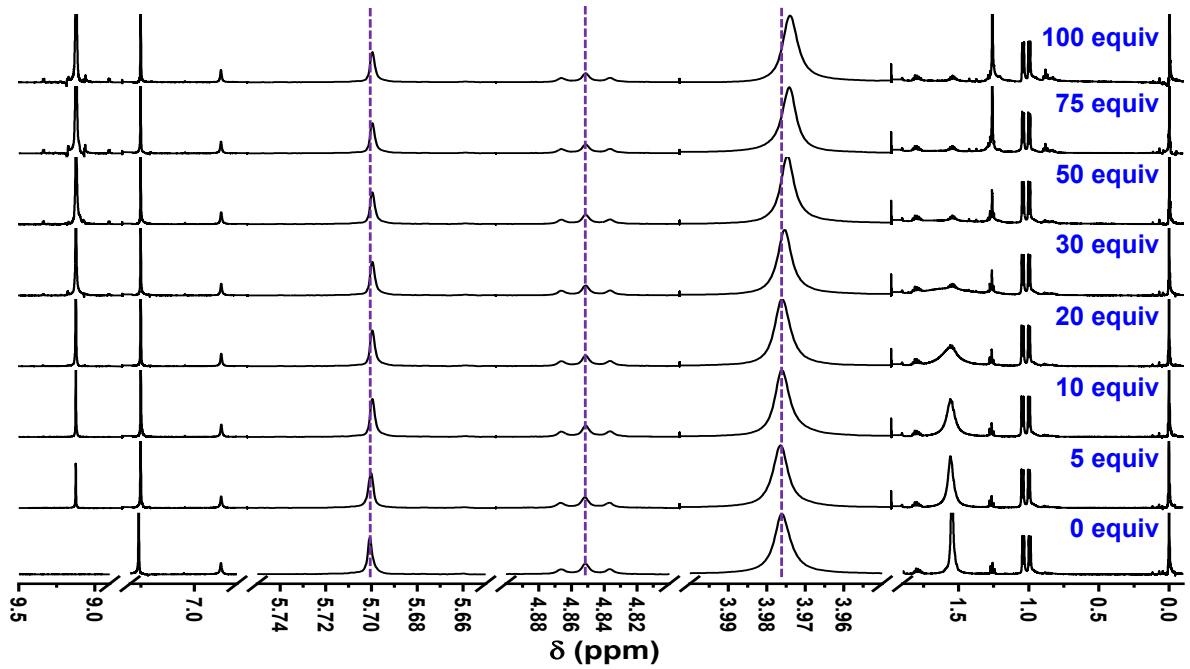

Fig S42: ^{1}H NMR titration results of **1b** against picric acid (0 – 100 equiv.).

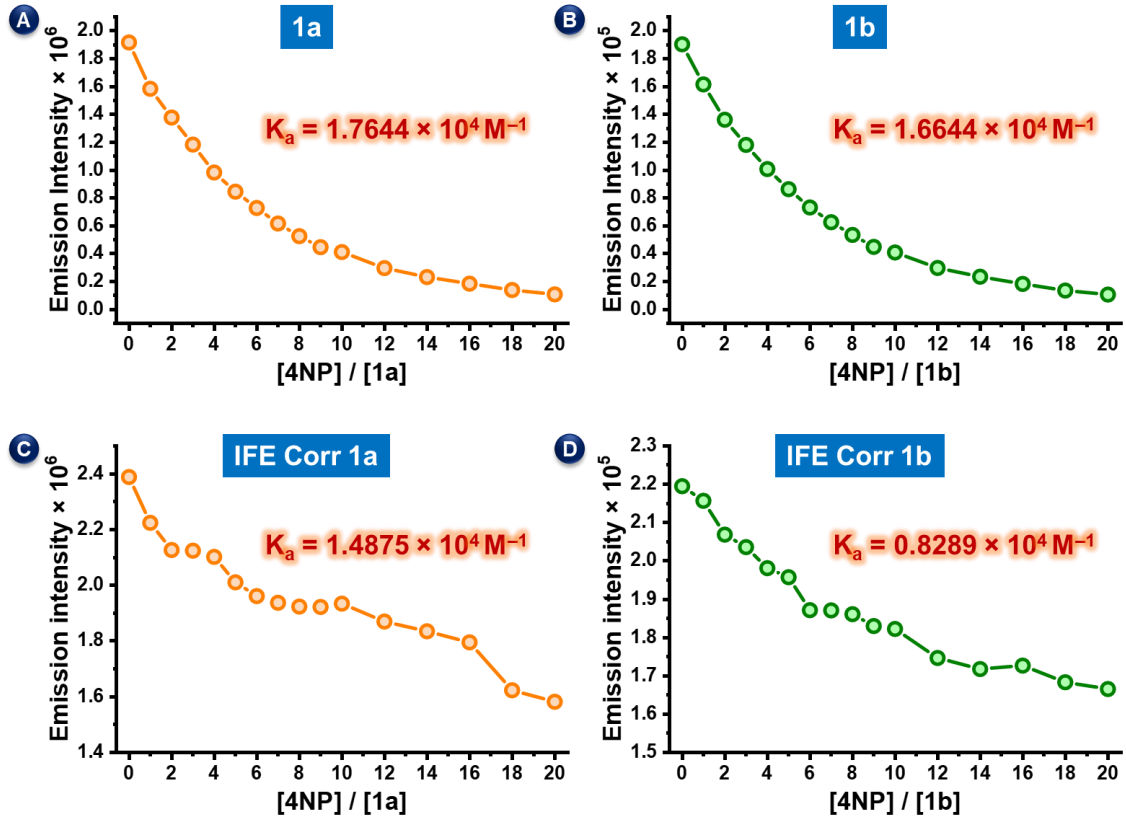

Figure S43: Binding constants extracted from the fluorescence emission intensity changes @461 nm for **1a** (A) and @454 nm for **1b** (B) vs the equivalents of 4NP, and the IFE corrected binding constants of **1a** (C) and **1b** (D).

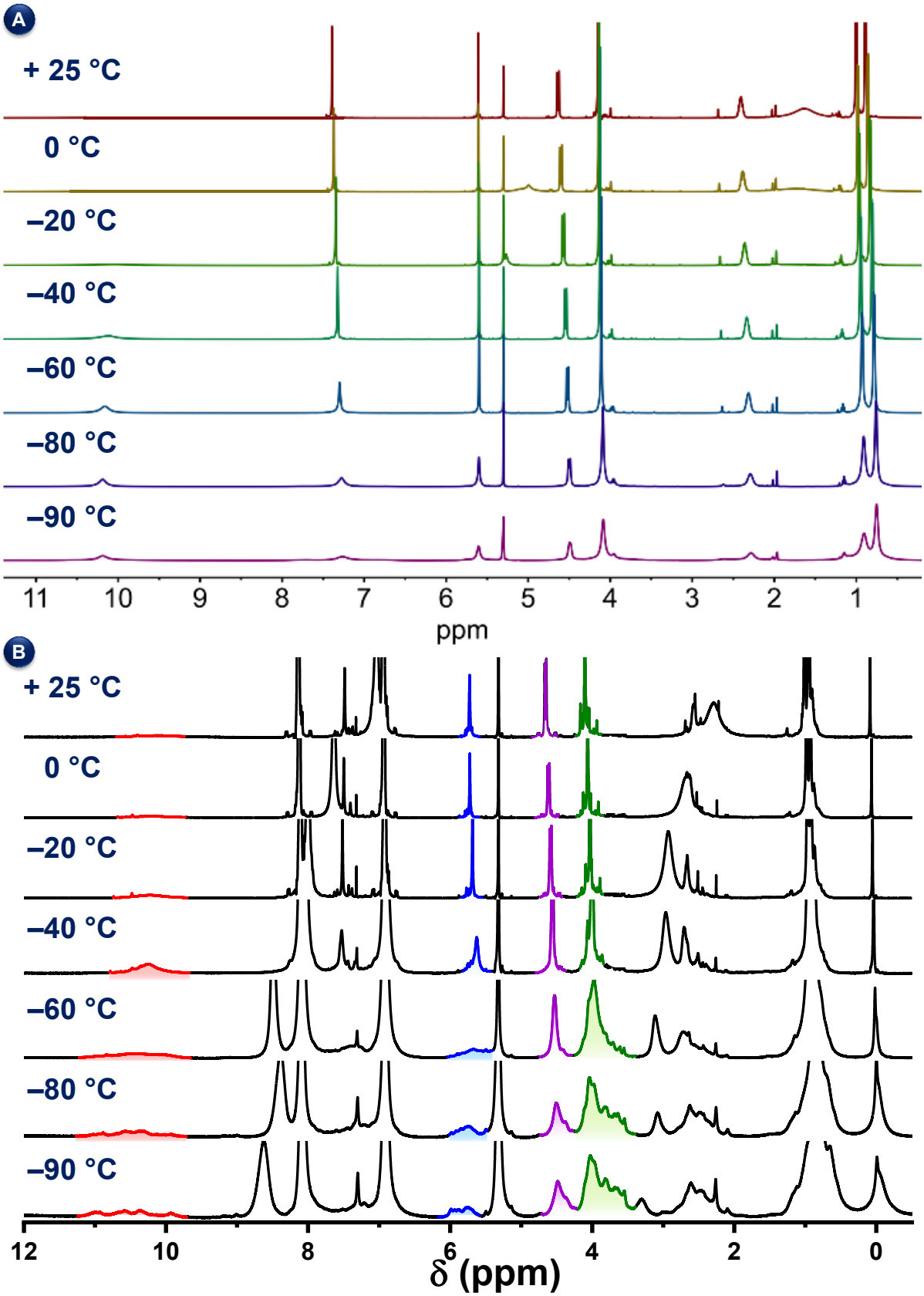

Fig S44: Variable low-temperature ^{1}H NMR spectra of **1a** (A) and a 1:10 mixture of **1a**:4-nitrophenol (B) in DCM-D_2.

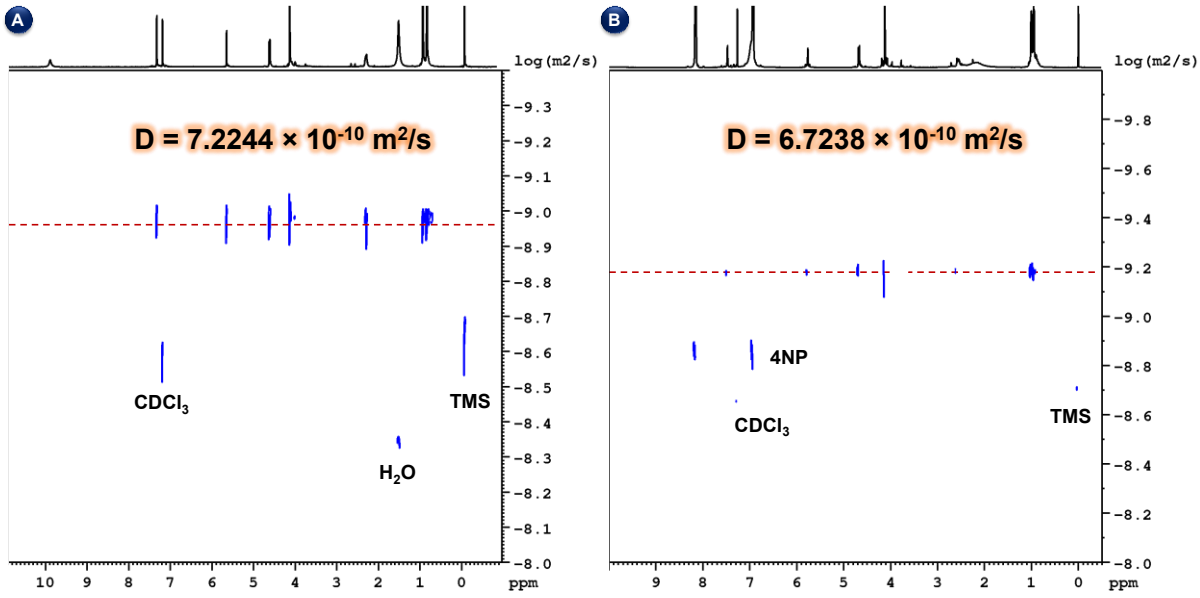

Fig S45: ^{1}H DOSY spectra of **1a** (A) and a 1:10 mixture of **1a**:4-nitrophenol (B) in $CDCl_3$.

Calculation of the Hydrodynamic radii from the diffusion coefficient:

We have calculated the hydrodynamic radii using the Stokes-Einstein equation.

$$D = \frac{k_B T}{6\pi\eta R_h} \qquad \text{Eq 1}$$

where,

D = diffusion coefficient (in m^2/s),

k_B = Boltzmann constant (1.38×10^{-23} J/K),

T = absolute temperature (in Kelvin),

η = is the viscosity of the solvent (in Pa·s),

R_h = hydrodynamic radius (in meters).

If we rearrange equation 1

$$R_h = \frac{k_B T}{6\pi\eta D} \qquad \text{Eq 2}$$

*Calculation of R_h for the macrocycle **1a**:*

D = 7.22 × 10^{-10} m^2/s.

k_B = 1.38 × 10^{-23} J/K,

T = 298 K

η = 0.54 centipoise ➔ 0.00054 Pa*s, (Viscosity of $CDCl_3$)

Substitute all values in equation 2

$$R_h = \frac{(1.38 \times 10^{-23}) \times 298}{6 \times 3.14 \times 0.00054 \times (7.22 \times 10^{-10})}$$

$$R_h = \frac{(1.38 \times 10^{-23}) \times 298}{6 \times 3.14 \times 0.00054 \times (7.22 \times 10^{-10})}$$

$$R_h = \frac{4.115 \times 10^{-21}}{7.342 \times 10^{-12}} = 5.6 \times 10^{-10}\ m$$

$$\boldsymbol{R_h = \sim 5.6}\ \text{Å}$$

*Calculation of R_h for the supramolecular complex 4NP@**1a**:*

D = 6.72 × 10^{-10} m^2/s.

k_B = 1.38 × 10^{-23} J/K,

T = 298 K

η = 0.00054 Pa*s,

Substitute all values in Equation 2

$$R_h = \frac{(1.38 \times 10^{-23}) \times 298}{6 \times 3.14 \times 0.00054 \times (6.72 \times 10^{-10})}$$

$$R_h = \frac{(1.38 \times 10^{-23}) \times 298}{6 \times 3.14 \times 0.00054 \times (6.72 \times 10^{-10})}$$

$$R_h = \frac{4.115 \times 10^{-21}}{6.825 \times 10^{-12}} = \sim 6.0 \times 10^{-10}\ m$$

$$\boldsymbol{R_h = \sim 6.0\ \text{Å}}$$

Experimental Details on the Filter paper/TLC-based detection of 4NP

Stability: The emission of the macrocycle on both filter paper and TLC plates remained stable at room temperature for more than a week, and even after exposure to 4-nitrophenol (4-NP). Thermal stability tests were performed by heating the samples at 40, 60, 80, and 100 °C (1 h each), both before and after 4-NP exposure. The fluorescence emission was retained even after heating to 100 °C, confirming excellent thermal and environmental stability of the sensing platforms.

Salt and pH Variation: To evaluate practical applicability under real conditions, 4-NP detection was also tested in brine solution, 0.01 M HCl (pH = ~ 2), and 0.01 M Na_2CO_3 (pH = ~ 11). The macrocycle maintained its sensing ability under all these conditions, demonstrating its robustness toward ionic strength and pH variations.

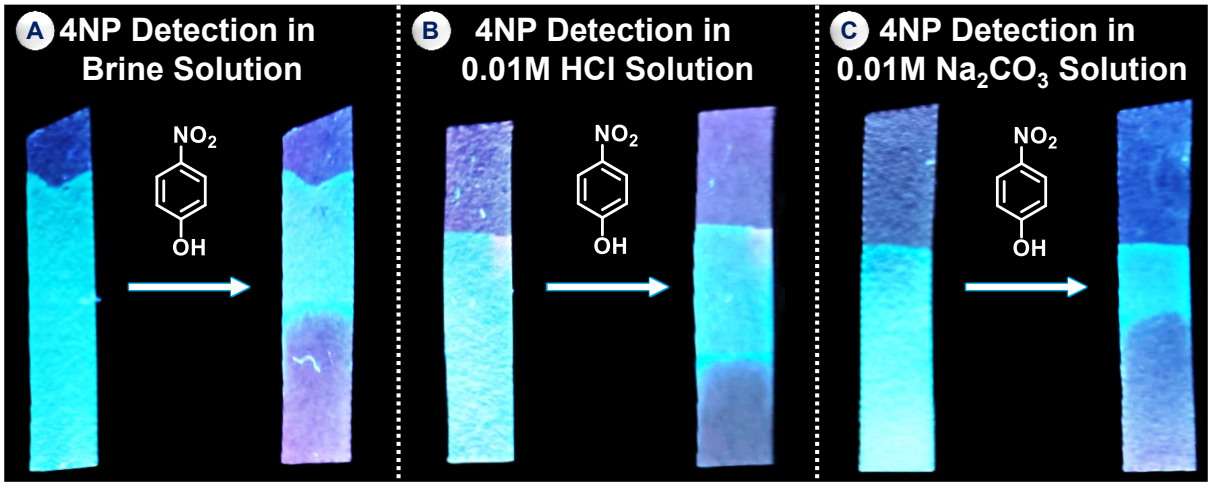

Figure S46: Filter paper detection of 4NP by **1a** in brine solution (A), 0.01 M HCl solution (pH ~2) (B), and 0.01 M Na_2CO_3 solution (pH ~11) (C) under UV light (λ_{ex} = 350 nm).

Reusability: For reusability studies, the filter paper strips tested with 4-NP were washed with water, acetonitrile, and ethanol solvents. However, the emission

could not be recovered, indicating strong binding of 4-NP with macrocycle **1a**, and thus a single-use (disposable) sensor format. Interestingly, the TLC plate-based system showed restoring the emission of the macrocycle **1a**, upon elution with 20% ethyl acetate/hexane, 4-NP (R_f = 0.36) moved up the plate, which demonstrating the reversible detection on TLC.

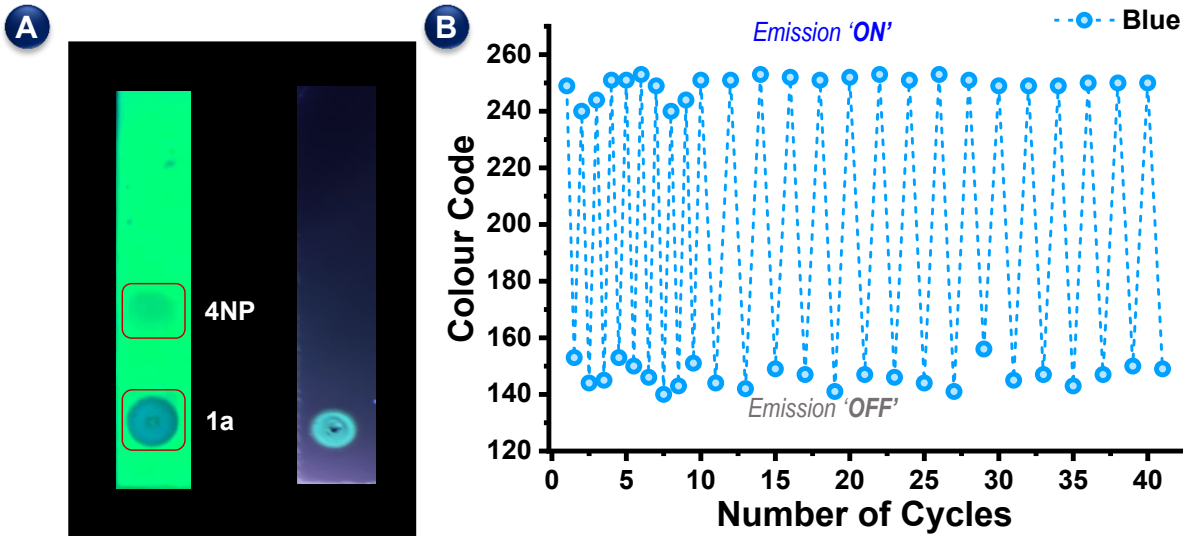

Figure S47: (A) Photographs of the eluted TLC (20% ethyl acetate/hexane) and blue-emission regeneration of **1a** under UV light (λ_{ex} = 350 nm). (B) Colour code of blue extracted from the photographs of the quenched (OFF) and regenerated (ON) emissions of **1a** for 40 ON-OFF cycles.

Reproducibility: All sensing experiments, including the filter paper and TLC plate assays, were performed at least three times, and the presented data and images represent the average and most reproducible results, confirming the reliability and repeatability of the method. The above TLC-based method indicates 40 repeatable cycles demonstrating recyclability and reproducibility of the platform.

Table S1. Performance comparison of macrocycles for nitroaromatic sensing.

Entry	Sensor Molecule	Analyte	LOD	Binding Constant	Naked Eye Detection	Medium	Ref.
1	β-CD-capped CdTe QDs	2-/3-/4-Nitrophenol	*o*-/*p*-NP: 0.05 μM *m*-NP: 0.3 μM	Not specified	No	Water	4
2	β-CD capped ZnO QDs	4- Nitrophenol	0.34 μM	Not specified	No	Water	5
3	ASPT-β-CD supramolecular fluorophore	4- Nitrophenol	0.01 μM	Not specified	Yes	Water	6
4	HP-β-CD modified Sulphur QDs	4- Nitrophenol	0.25 μM	Not specified	Not reported	Water	7
5	Cucurbit[8]uril-based (G@Q[8])	2- Nitrophenol	0.015 μM	3.52×10^6 M^{-1}	Yes	Water	8
6	TPP-DMB Conjugated Hyper-crosslinked Polymer	4- Nitrophenol	Not explicitly reported (high sensitivity)	1.31×10^4 M^{-1}	Yes	THF	9
7	Tetraphenylethylene (TPE) Conjugates (AIE-active)	Nitro-explosives (TNT, TNP, RDX, DNT, etc.)	Varies, generally ultra-trace levels	Not specified	Not clearly reported	Water	10
8	HOF-TPE-CN (Hydrogen-bonded organic framework)	2-/3-/4-Nitrophenol	0.65 μM	Not specified	No	Water	11
9	Pillar[5]arene-based Cu(II) supramolecular aggregate	4-Nitrophenol	0.39 μM	Not specified	Yes	Water	12
10	Coumarin[4]arene macrocycle	4-Nitrophenol	6.9 μM Up to 10^{-8} M	$0.83–1.49 \times 10^4$ M^{-1}	Yes, Filter paper strip, TLC @ RT to 100 °C	CH_3CN, Water, brine, acid and base media	This Work

References

1. P. Kumar, P. Venkatakrishnan, *Org. Lett.*, 2018, **20**, 1295−1299;
2. P. Kumar, P. Venkatakrishnan, *Eur. J. Org. Chem.*, 2019, 7787–7799.
3. P. Kumar, V. B. RajaManiKandan,. P. Balakrishnan, P. K. S. Antharjanam, and V. Parthasarathy, *Angew. Chem. Int. Ed.*, 2023, e202305005.
4. Z. Zhang, J. Zhou, Y. Liu, J. Tang and W. Tang, *Nanoscale*, 2015, **7**, 19540–19546.
5. S. Geng, S. M. Lin, S. G. Liu, N. B. Li and H. Q. Luo, *RSC Adv.*, 2016, **6**, 86061–86067.
6. Z. Zhang, F. Fang, P. Zhang, X. Zhang, H. Ma and Y. Wei, *Colloids Surf. Physicochem. Eng. Asp.*, 2024, **695**, 134087.
7. Y. Chang, R. He, R. Wang, Y. Wei and L. Wang, *J. Mater. Chem. C*, 2024, **12**, 14605–14612.
8. J. He, X.-Y. Yu, Z.-C. Yu, M. Liu, P.-H. Shan, C. Redshaw, Y. Huang, Z. Tao and X. Xiao, *Anal. Chim. Acta*, 2022, **1226**, 340262.
9. Y.-C. Wang, F. Zhu, J.-Y. Zhang and T.-M. Geng, *Microchem. J.*, 2025, **209**, 112739.
10. M. Majid, M. Amin, K. Bashir, W. A. Wani, J. Ahmad Rather, F. Habib, W. Ahmad Khanday, M. Syed Shah, A. Hussain Malik and M. A. Yatoo, *J. Ind. Eng. Chem.*, 2025, **143**, 109–122.
11. Y.-X. Lin, C. Jiang, Y.-B. Wang, J.-X. Wang, B. Li and G. Qian, *J. Mater. Chem. A*, 2024, **12**, 153–161.
12. D. Yu, W. Deng and X. Wei, *Dyes Pigments*, 2023, **210**, 110968.

****